CHALMERS
UNIVERSITY OF TECHNOLOGY

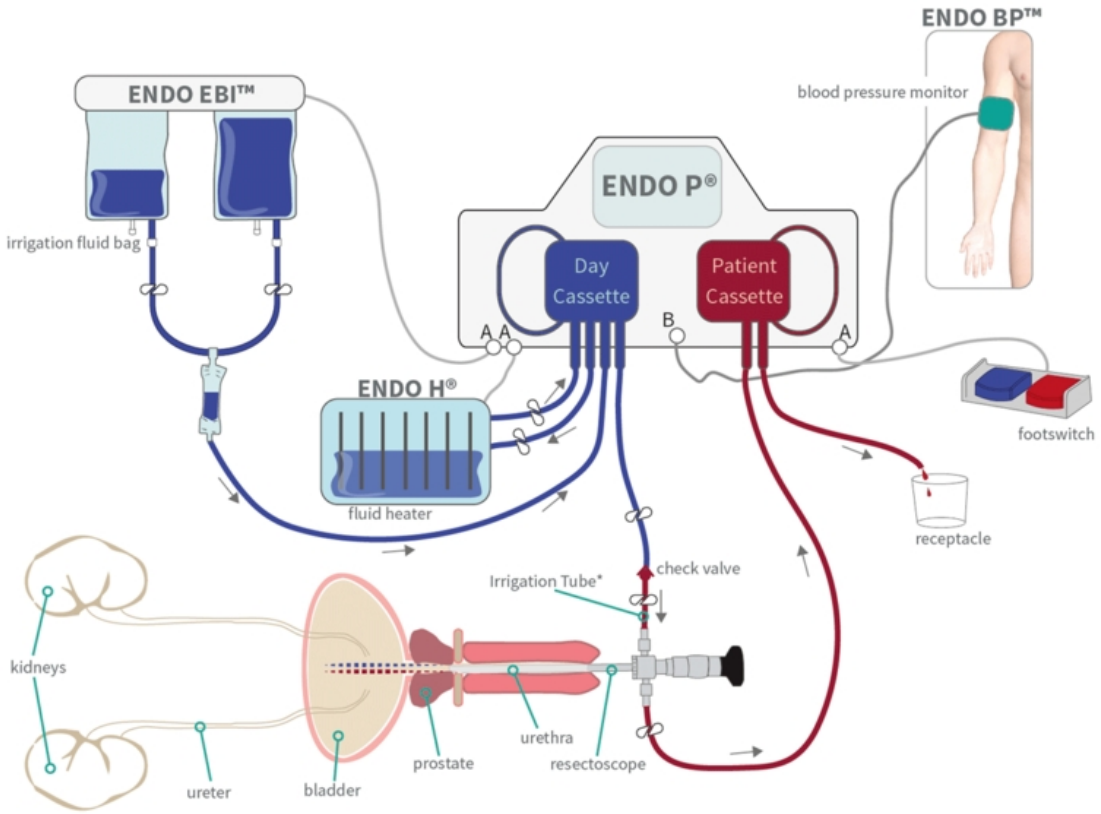

Control Algorithm and Graphical User Interface for Endoscopic Surgery Pump

Control Algorithm Proposal and GUI Design for ENDO P®

Master's thesis in Systems, Control and Mechatronics

IVANA IVKOVIĆ

Department of Signals and Systems
CHALMERS UNIVERSITY OF TECHNOLOGY
Gothenburg, Sweden 2015

Master's thesis 2015: EX038/2015

Control Algorithm and Graphical User Interface for Endoscopic Surgery Pump

Control Algorithm Proposal and GUI Design for ENDO P®

IVANA IVKOVIĆ

Department of Signals and Systems
Division of Control, Automation and Mechatronics
Chalmers University of Technology
Gothenburg, Sweden 2015

Control Algorithm and Graphical User Interface for Endoscopic Surgery Pump
Control Algorithm Proposal and GUI Design for ENDO P®
IVANA IVKOVIĆ

Supervisor: Marco Monzani, Bonvisi AB
Examiner: Balázs Adam Kulcsár, Assistant Professor, Department of Signals and Systems

Master's Thesis 2015: EX038/2015
Department of Signals and Systems
Division of Control, Automation and Mechatronics
Chalmers University of Technology
SE-412 96 Gothenburg
Telephone +46 31 772 1000

Cover: Connection diagram of ENDO P® with the accessories at the operating site.
Source: http://www.bonvisi.com/products/endop.html Accessed: 15.05.2015.

Typeset in LaTeX
Printed by [Name of printing company]
Gothenburg, Sweden 2015

Control Algorithm and Graphical User Interface for Endoscopic Surgery Pump
Control Algorithm Proposal and GUI Design for ENDO P®
IVANA IVKOVIĆ
Department of Signals and Systems
Chalmers University of Technology

Abstract

Minimally invasive surgeries are one of the fastest growing medical fields today because of patient benefits such as faster recovery and reduced risk of infection. But minimally invasive surgeries are quite challenging for the surgeon to perform because of reduced maneuvering space and visibility. Therefore more and more technological solutions are developed to aid the surgeon in this task. ENDO P® is an endoscopy pump designed to improve visibility, maintain the pressure in the operating cavity and prevent fluid uptake which can, in severe cases, be fatal for the patient. This thesis aims to investigate different control strategies and graphical user interface that could be used by the ENDO P® system and their effects on surgery safety, duration and efficiency. The system was analyzed and modeled based on fluid dynamics, mechanics and system identification. A Simulink model was built and three different control algorithms: the state machine like zone bang-bang strategy, PID control and structured robust control were compared in the simulation environment. Based on the best simulation result, complexity, reliability and ease of implementation, robust structured method provided the best overall controller. During the simulated surgery the controller showed robust performance against perturbations with steady control variable value and good reference tracking. GUI designed was proved to be intuitive and well in sync with the surgery flow. These results can serve to strengthen the case for use of ENDO P® in endoscopic surgeries in urology compared to traditional methods, and confirm the benefits of controlled pressure for the patients safety.

Keywords: ENDO P®, endoscopic surgery, pressure control, biological system modeling, $\mathcal{H}_\infty$ structured controller

Acknowledgements

I would like to thank my supervisor Marco Monzani and my examiner Balázs Adam Kulcsár for professional guidance and pointing me in many academically and practically challenging directions. I would also like to thank Anders Möllstam for his expert insight on the subject. Special thanks goes to my colleges Charul Sampath, Mathias Ernst and Samuel Scheidegger for being excellent opponents and starting interesting discussions. I would also like to thank my college and friend Vilim Štih, who was especially helpful with his constructive criticism and impressive encyclopedia knowledge. Thanks to Arundhati and István for wonderful company and positive attitude and all my friends who were a great support. Finally I would like to thank Bonvisi AB for the opportunity to perform this highly rewarding work.

I would like to dedicate this thesis to my sister who still has a long way to go, to my nona who taught me all the important things, to my Lana who inspired me, and to my mother who made all this possible. Thank you.

Ivana Ivkovic, Gothenburg, June 2015

Contents

List of Figures **x**

1 Introduction **1**
1.1 Purpose and challenges . . . 1
1.2 Method and material . . . 3
1.3 Thesis structure . . . 3

2 Clinical problem **5**
2.1 Endoscopy in urology . . . 5
2.2 Current practice and complications . . . 6
2.3 ENDO P® - solutions and benefits . . . 7

3 Model of the system **9**
3.1 ENDO P® technology . . . 9
3.2 Mathematical model . . . 12
3.3 Subsystems . . . 14
3.3.1 Pumps . . . 15
3.3.2 Sensors . . . 16
3.3.3 Tubing . . . 17
3.3.4 Bladder . . . 21
3.3.4.1 Pressure–stretch curves . . . 21
3.3.4.2 Simple nonlinear model . . . 23
3.3.4.3 Uncertain linear model . . . 25
3.4 Simulink® model . . . 28

4 Control design **29**
4.1 Zone bang-bang (finite state machine) . . . 30
4.1.1 Theory . . . 30
4.1.2 Simulation results . . . 31
4.2 PID . . . 35
4.2.1 Theory . . . 35
4.2.2 Simulation results . . . 36
4.3 $\mathcal{H}_\infty$ structured control . . . 38
4.3.1 Theory . . . 39
4.3.2 Modeling . . . 41
4.3.3 Simulation results . . . 43
4.4 Controller suggestion . . . 45

5 Implementation **49**
5.1 Test system setup 49
5.2 Bottle model 49
5.3 Controller comparison 50

6 Graphical User Interface design **53**
6.1 Procedure flow 53
6.2 Design choices 55

7 Conclusion **61**

Bibliography **63**

A Appendix **I**

List of Figures

3.1 ENDO P® front view. Tubing ports on the cassettes are marked with arrows. Pressure sensors locations are marked with blue circles. . . . 9

3.2 ENDO P® back-panel with ports for power supply, programming, pedal input and accessories. 10

3.3 ENDO Pump™ System 11

3.4 Pressure drop diagram. p_c marks the cavity pressure, Δp_{ti} and Δp_{to} are dynamic pressure drops in the tubing and p_{mi} and p_{mo} are pressures measured at sensors. Δh is the difference in height between the cavity and the device affecting the hydrostatic pressure. 14

3.5 Peristaltic pump with three rollers. As the central part rotates, rollers compress the clamped tubing pushing the liquid in the direction of rotation. 15

3.6 Inflow pump model. Input disturbance models the uncertainty connected with pump model identification. Pressure influence models the overall system pressure influence on the delivered flow. Both input u and output y of the subsystem are flows [ml/min]. 16

3.7 Sensor model. At the output of the sensor dynamics block the colored noise is added to simulate the disturbances. Both input and output of the sensor model subsystem are pressures [mmHg]. 17

3.8 Tubing model. Static pressure drop and uncertainty model the height difference influence and the transfer function T and uncertain dynamics model the flow dependent dynamic pressure drop. Inputs to the tubing model are static pressure drop [mmHg] and flow [ml/min]. The output of the tubing model is pressure [mmHg] added to the bladder pressure to compensate for pressure drops in the tubing. 20

3.9 Monkey bladder pressure-stretch curve. Blue curve is the monkey bladder data adapted from Osborne and the red curve is the fitted Mooney model with parameters: $C_1 = 31.75$, $C_2 = 0.28$, $n = 6.05$. . . 22

3.10 Parameters a and b of the power function. Left figure shows the parameter a trend following radius increments. Right figure shows parameter b linear dependence on radius increments. Red circles are sampled points. 24

3.11 Bladder models with different radius. Each line represents a single bladder model with different maximum radius. Higher radius means larger bladder volume. 24

3.12 Uncertain linear model of the bladder. Considering the slopes of the nonlinear bladder models two red circles mark the chosen linearization points that produce the two linearised models that limit the uncertain state space. 27

3.13 Simulink® model of the system 28

4.1 Zone bang-bang: control signal values. Outflow (blue) is kept constant and inflow (red) is varied to control pressure. Differences in flows are larger as the error is further from zero to make the effect of pressure drop or rise faster. 31

4.2 Zone bang-bang: simulated control signal values. Outflow (blue) is the reference flow and the inflow control signal (red) spikes coincide with pressure reference changes and disturbance rejection. 32

4.3 Zone bang-bang: measured pressure and reference. Measured pressure is the pressure visible on the sensors of the system consisting of the bladder pressure, pressure drop in tubing and disturbances. . . . 32

4.4 Zone bang-bang: cavity pressure and reference. Cavity pressure is not directly measured and can only be observed in the simulation environment. 33

4.5 Oscillations in the cavity pressure. Magnified part of the figure 4.4 overlaid with the inflow control signal to demonstrate the effect of the unsteady inflow. Ripples in the cavity pressure match the period of those introduced by inflow. 34

4.6 Zone bang-bang: system uncertainty influence on cavity pressure. Five different random simulations are presented. 34

4.7 PI with anti-windup. K_p and K_i are tunable parameters of the controller. Anti-windup scheme implemented is conditional integration. 36

4.8 PI: control signal values. Outflow (blue) is the reference flow and the inflow control signal (red) spikes coincide with pressure and flow reference changes and disturbance rejection. 37

4.9 PI: measured pressure and reference. Measured pressure is the pressure visible on the sensors of the system consisting of the bladder pressure, pressure drop in tubing and disturbances. 37

4.10 PI: cavity pressure and reference. Cavity pressure is not directly measured and can only be observed in the simulation environment. Spikes at times 20 min and 40 min are a consequence of internal disturbances of the bladder model. 38

4.11 PI: system uncertainty influence on cavity pressure. Five different random simulations are presented. 38

4.12 Closed loop system. w are disturbance inputs, u are controlled inputs, z are controlled outputs and y are measured outputs. 40

4.13 Augmented linear plant. Uncertain inputs together with $d(t)$, $n(t)$, $rf(t)$ and $rp(t)$ represent disturbance inputs, controlled input is $u(t)$ and the measured output is $e(t)$. The rest of the outputs are controlled outputs. Augmented system does not represent the real system but rather the adjusted system with added filters needed for control synthesis. 42
4.14 $\mathcal{H}_\infty$: control signal values. Outflow (blue) is the reference flow and the inflow control signal (red) spikes coincide with pressure reference changes and disturbance rejection. 43
4.15 $\mathcal{H}_\infty$: measured pressure and reference. Measured pressure is the pressure visible on the sensors of the system consisting of the bladder pressure, pressure drop in tubing and disturbances. 44
4.16 $\mathcal{H}_\infty$: cavity pressure and reference. Cavity pressure is not directly measured and can only be observed in the simulation environment. Small pressure spikes noticeable at times 20 min and 40 min are a consequence of internal bladder model disturbances. Spikes at times 13 min, 26 min, 39 min and 52 min are caused by flow reference changes. 45
4.17 $\mathcal{H}_\infty$: system uncertainty influence on cavity pressure. Five different random simulations are presented. 45
4.18 System responses to the 60 mmHg reference. Flow reference changes at times 10 min, 20 min and 30 min. Internal system disturbance occurs at 20 min. 46
4.19 System control signals compared. Stable pressure reference of 60 mmHg is maintained. 47

5.1 Test system responses with different controllers. The pressure reference signal is kept constant at 70 mmHg and the flow reference signal is kept constant at 200 ml/min. The saturation parameters for the PI controller are 300 ml/min and 50 ml/min. 0 mmHg pressure is not the starting pressure due to digital sensor imperfections and the dead time of each response is a consequence of human response time, since it takes some time from starting the pressure recording process to starting the ENDO P®. 50
5.2 Test system response compared to the simulation. The pressure reference signal is kept constant at 70 mmHg and the flow reference signal is kept constant at 200 ml/min. PI controller is used. 51

6.1 Diagnostic screen. Left: Screen expecting the operator to preform the highlighted action. Right: Screen prompting the operator to tap the play button on the screen. 55
6.2 EBI™ Diagnostic screen addition. 55
6.3 Settings screen. Left: By taping on the numbers the screen brightness and system volume can be adjusted. Right: Language selection part of the settings screen. 56
6.4 Manual height calibration screen. Left: Height to patient or height to ENDO P® can be selected. Right: The selected and highlighted is entered by tapping on numbers. 56

6.5 Main screen. Central screen leading to surgery selection, height recalibration, priming and surgery run screen. 57
6.6 Priming procedure screens. Left: Safety screen preventing an unintended start of the priming procedure. Right: Priming procedure screen displaying the current flow. 57
6.7 Automatic height calibration and procedure selection screens. Left: Automatic height calibration screen displaying the currently measured patient height. Right: Procedure selection screen. Procedures are selected by taping the wanted procedure button. 58
6.8 Run screen. Screen visible during ongoing surgery. Standby is the only active button. Values are displayed to inform the surgeon about the surgery conditions. 58

1

Introduction

The trend toward minimally invasive surgery, in the medical world today, is a well established fact. Reducing loss of blood and tissue damage, as well as the risk of infections, by executing smaller incisions is a primary goal. Additional benefits of faster recovery, shortened hospital stay and minimal scarring make them a popular choice with the patients worldwide.

Minimally invasive surgeries can be quite challenging and technically demanding for the surgeon. Introducing and maneuvering instruments through small incisions requires special training and precision. Also, possible complications during the surgery are much more difficult to control and resolve. To increase safety of the procedure and assist the surgeon, different technologies are developed and introduced. Optical and video equipment for increasing visibility and robotic arms for precision are just some of the examples.

This thesis deals with the new and innovative technology of pressure control for minimally invasive endoscopic surgeries in urology. The new urology pump ENDO P® simplifies operations in the prostate and other parts of the urinary tract through a patented method developed by the medtech company Bonvisi [1]. Endoscopy requires a fluid to be pumped through the operating cavity in which the operation takes place. The flow of this fluid, if properly regulated, guarantees optical clearance for the endoscope and, by counteracting the blood pressure, reduces the bleeding. The endoscopy pump regulates the fluid flow during the operation, controlling the pressure in the operating cavity, making the procedure safer, faster, more efficient and less expensive.

1.1 Purpose and challenges

The purpose of this master thesis is to aid the development of ENDO P® urology pump by designing an intuitive, clear and user friendly graphical user interface and to investigate how the control algorithm of such a device could operate, having in mind the various requirements behind the specific application case. It is important to underline that this work was done on a pure speculative basis, and, even if the case is based on a real device, the academical and research values were prioritized.

Challenges include: understanding the clinical problem and the requirements for device operation; building a model of the system consisting of a highly variable and uncertain model of operating environment, namely the operating cavity, which is dependent on biological parameters such as bladder volume and muscle fatigue; devising a simple and reliable control strategy that will not be computationally demanding for the hardware and that will not be too reliant on the uncertain model; comparing simulated performance of different control strategies as a means of finding the best suited one for this application and incorporating user feedback to the GUI design idea.

Thus this thesis aims to:

1. Introduce the clinical problem and standard operation procedures;
2. Present the ENDO P® technology and explain expected benefits of using such a device;
3. Analyze the system consisting of ENDO P®, tubing and the operating cavity and devise a representative model of each subsystem;
4. Present three different control strategies for this particular application: zone bang-bang controller (finite state machine approach), PID controller and structured $\mathcal{H}_\infty$ robust controller;
5. Compare the simulations and evaluate controller performance;
6. Provide an intuitive, informative and non-distracting design for graphical user interface.

Finally, this thesis aims to investigate which is the most applicable control algorithm for controlling nonlinear systems with unknown dynamics and time varying parameters, such as the surgical cavity during endoscopic operation using ENDO P®.

When controlling biomedical systems dependent on physiological parameters it is impossible to take into account all the contributing factors and precisely model the ongoing processes, especially because a lot of the parameters are time varying and their periods are highly subjective. Due to high uncertainty in such models it is worth researching different control strategies. Is it better to just apply the simple feedback and react to the changes or try to develop a more sophisticated algorithm which will take into account at least some of the system dynamics? Which algorithm is more responsive? Which is safer and less prone to failure? Which stabilizes the system for a wider range of disturbances? In answering these questions, this thesis will give rise to intuition regarding control algorithms for biomedical systems and will be a good starting point for further research concerning biomedical systems control.

1.2 Method and material

Preceding any work on this thesis, a literature review was conducted to better understand the challenges and requirements of the clinical problem. An interview with the experienced professional, Anders Möllstam, gave good insight at how the specific urology endoscopic surgeries are preformed in practice and what complications may arise.

The idea and technology behind the new urology pump ENDO P® was studied in detail. This device was developed by Bonvisi AB, a privately owned Swedish medtech company located in Stockholm. Since at the start of the thesis the device was not yet released, part of the work was conducted at the manufacturing site in Ashford, England.

From discussions about the flow of surgery and the ENDO P® sequence of operation, a design for GUI done in Inkscape [2] was proposed and revised based on user feedback.

For the control part, static model of the specific subsystems was identified from the data gathered through the series of tests conducted on the test site. Some parts of the system were modeled by black box approach, and some, after the consultation with the literature, as gray box with uncertain parameters. Data processing, modeling and simulation of the system and control design were done in MATLAB® [3] and Simulink® [4].

The choice of the appropriate controller was made based on requirements such as safety, low complexity, low computation demand, good reference tracking, rise time, stability, control signal and high adaptability to uncertainties in the model.

1.3 Thesis structure

This thesis is arranged so that the first chapter *Introduction* gives short overview of the goals and lays out the framework thesis will follow.

In the second chapter *Clinical problem* is presented together with current standard practices in endoscopic urology. Brief explanations of the procedures and most common complications are given.

The third chapter *Model of the system* focuses on the innovative technology of the ENDO P®, solutions such technology provides, system identification and mathematical modeling of the device elements and functions.

The forth chapter *Control design* presents the theory and reasoning behind the chosen control algorithms, gives guidelines for their MATLAB® implementation

and compares their performance on the system model in the Simulink® simulation environment.

The fifth chapter *Implementation* introduces implementation results obtained from the test system especially setup for this application.

The sixth chapter *Graphical User Interface design* is dedicated to GUI design and the final chapter *Conclusion* presents conclusions and points to possible further developments.

Bibliography lists the literature used for research and in the *Appendix* MATLAB® code of the system model and the controllers is attached.

2

Clinical problem

Development and introduction of the new technologies in medicine allowed for the fast and still continuing development of the minimally invasive procedures. Such procedures became common in almost all surgical fields, ranging from neurological, cardiac and vascular, to gastrointestinal, urology and orthopaedic surgeries. Due to the patient benefits such as less pain, less trauma, less blood loss, faster recovery, smaller skin scars, shorter hospital stay and smaller possibility of post surgical complications such as infections, this new field is only expected to grow in the future and replace open surgeries as standard practice for many surgical procedures.

Minimally invasive surgery refers to operative procedures performed by entering the skin through the smallest possible incision or through a body cavity or anatomical opening to reduce body trauma and damage to skin and muscles. Such operative procedures are quite complex, so specialist training and equipment such as fiber optics, cameras, different manipulators like instruments with handles or robotic arms are necessary.

2.1 Endoscopy in urology

Endoscopy is a minimally invasive procedure where an instrument equipped with optics, camera and light source, called endoscope, is inserted into the body cavity for effective visualisation of the interest area. In urology endoscopic procedures are used to diagnose and treat the problems with urethra, prostate, bladder and ureters. The endoscope is inserted through urethra and is used to extract tissue for biopsy, remove growths or cut out the diseased or damaged tissue. It consists of wide angle microscope, lighting system and a camera to display the magnified and illuminated structures inside the urinary tract on a monitor, irrigation and evacuation channels to flush the cavity and evacuate blood and tissue, and a port for electrodes used in form of a wire loop that cut and cauterize the tissue.

Procedures that are of interest for this thesis because of possibility for ENDO P® use are: TUR-P (transurethral resection of the prostate), TUR-B (transurethral resection of the bladder), Ureter (surgery in between bladder and kidney), Kidney (surgery in the upper end of the ureter) and Cystoscopy (diagnostic procedure for

investigating the urinary tract).

TUR-P or transurethral resection of the prostate is the most common procedure and it is preformed in case of benign prostatic hyperplasia (BPH). BPH is a benign enlargement of the prostate that can cause obstructions in the urethra and lead to obstruction of the urine stream, incontinence, bladder deformations, higher risk of urinary tract infections and even kidney failure. TUR-P procedure is also used in prostate cancer biopsy as well as treatment in early stages. TUR-B or transuretral resection of the bladder is used for bladder cancer treatment, while Urethra and Kidney are used for Urethral stricture and Urolithiasis or removal of the kideny stones.

2.2 Current practice and complications

Even though different operating conditions are necessary for different procedures, low and constant pressure during TUR-P, high flow rate for increasing visibility in TUR-B, high pressure during Urethral stricture and high flow rate with low pressure for Kidney procedure to avoid damage to the pressure sensitive kidneys, in practice today most prevalent method for these surgeries is gravity pressure and flow control.

The method consists of hanging sterile, 3 liter bags of irrigation fluid, usually saline or glycine, from a stand above the patient with tubing leading to the endoscope. Fluid then enters the operating cavity through the irrigation channel, flushes the site and evacuates through the evacuation channel. Gravity aids the flow of the fluid and the hydrostatic pressure provides approximate estimate of the operating pressure. Pressure and flow control are done by adjusting the height of the fluid bag on the stand.

The irrigation is very important in these procedures because it expands the operating cavity creating more maneuvering space, flushes away blood and debris, increasing visibility, and strives to keep the homeostasis at the operating site by compressing damaged veins to reduce bleeding. Challenges arise when the flow or the pressure of the irrigation fluid are insufficient. Too low pressure or flow in the operating cavity lead to bleeding, which blurs the lens of the endoscope and obstructs the procedure. To momentarily increase the flow it is common practice to squeeze the bags manually or by applying a blood pressure cuff. This results in both flow and pressure being increased in an uncontrolled way. High pressure intervals can damage the tissues and organs and can lead to the most dangerous complication called TUR-syndrome.

TUR-syndrome or transurethral resection syndrome is a complication most common in the prostate surgeries that happens due to high pressure at the operating site when the significant amount of irrigation fluid is forced into the blood stream through damaged blood vessels, diluting the blood. It can be identified by a number of symptoms that happen during or after the surgery like nausea, vomiting, headache, confusion, abdominal pain, respiratory problems, hypothermia, coma, cardiac arrest

etc. Mild to moderate TUR-syndrome may occur in 1–8% of patients with the mortality of 0.2–0.8%. Severe TUR-syndrome is rare; however, it carries a mortality of up to 25% [5].

To prevent the TUR-syndrome several methods are used. One method is to add a small amount of alcohol to irrigation fluid and monitor the amount of alcohol in patients exhaled breath. If alcohol is detected, fluid uptake occurred. Another method is to measure the length of surgery, or measure the weight of the extracted tissue. The longer the surgery the higher the possibility of fluid uptake, also the heavier the removed tissue, the larger the cut and blood vessel damage, therefore the possibility of TUR-syndrome increases. None of these methods are very reliable or precise but when there is a possibility of TUR-syndrome, surgery needs to be stopped regardless of the fact that not all cancerous tissue has been removed. This leads to further patient stress, repeated procedures, problematic recovery and additional costs.

2.3 ENDO P® - solutions and benefits

Main challenge in endoscopy in urology is to regulate the flow, ensuring good visibility throughout the procedure, and to regulate the pressure, ensuring minimal damage to tissue and preventing the irrigation fluid uptake. Furthermore it is important that both flow and pressure can be controlled independently.

In other medical fields, such as arthroscopy, this problem was solved using pumps. Some of these solutions such as Double® Pump from Medical Vision independently control inflow and outflow rates, decoupling flow from pressure, which means the operating cavity can be cleared of blood and debris without pressure spikes.

ENDO P® follows the same idea. Independently controlling in and out flow using two peristaltic pumps, optimal flow together with the desired pressure can be accomplished. Adjusting the flow enables good visibility and that is the prerequisite for continuing surgery. Thanks to the clear lenses the procedure can be done without interruptions and thus faster and without dangerous peak pressure that occurs when flow is increased manually. Steady flow also reduces the consumption of the expensive irrigation fluid.

Adjusting the operating cavity pressure to the perfusion pressure, the part of blood pressure that ensures blood flow, ENDO P® can help achieve optimal conditions for surgery, where both bleeding and fluid uptake are reduced to minimum. If the pressure in the cavity ENDO P® controls matches that of the blood vessels, homeostasis occurs and bleeding to the cavity together with the fluid migration from cavity to blood vessels is significantly reduced. With the less blood in the operating cavity, visibility is higher speeding up the surgery and lowering fluid consumption, on the other side, with less fluid in the blood, chances of TUR-syndrome decrease and operations need not be interrupted before all the tissue is removed.

By controlling the pressure ENDO P® greatly helps the surgeon preform the operation by increasing visibility and expanding the operating cavity for easier instrument manipulation, all the time offering the precise information about the flow and pressure inside the operating cavity and providing the estimate of the absorbed irrigation fluid volume. All this information aids the surgeon in making the procedure more efficient. It also makes the procedure much safer for the patient, reducing the operation time and the risks of TUR-syndrome, preventing tissue damage from high pressure, allowing faster recovery.

3

Model of the system

To develop a good control strategy, a model of the system is required. In the following chapter the technology of ENDO P® is presented and modeled to give rise to better understanding of the overall system and build a simulation platform for the developed algorithms. The greatest challenge however is to accurately model the biological system such as the human bladder, and to provide its representative linear model for control synthesis. Some of the choices made and the discussions to justify them are presented.

3.1 ENDO P® technology

Figure 3.1: ENDO P® front view. Tubing ports on the cassettes are marked with arrows. Pressure sensors locations are marked with blue circles.

In the figure 3.1 ENDO P® system is shown. It consists of the two peristaltic pumps, inflow (on the left) and outflow (on the right), responsible for delivering the flow to and from the operating cavity; large touchscreen display for setting up the procedure and interacting with the device; two cassettes, Day cassette (element

connected to the pump on the left) and Patient cassette (element connected to the pump on the right) used to interface pumps, tubing and pressure sensors. There is also an emergency stop switch (the red button) and the blood pressure monitor cuff port just beneath it. Both Day and Patient cassettes together with the tubing are disposable elements of the system. Day cassette should be changed daily, while Patient cassette should be changed with every patient to prevent contamination.

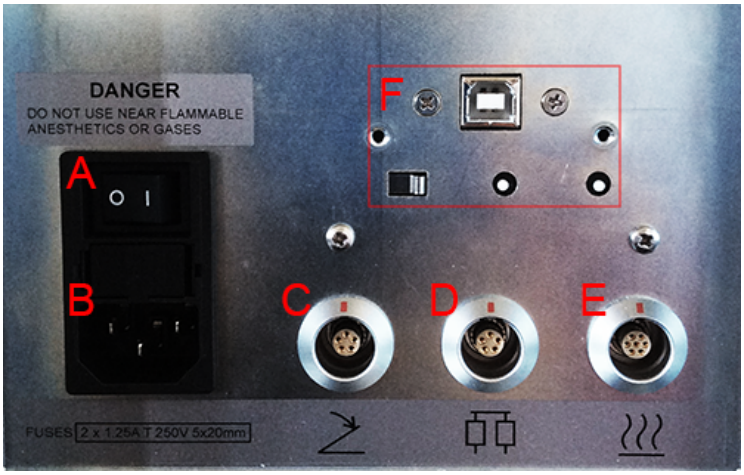

Figure 3.2: ENDO P® back-panel with ports for power supply, programming, pedal input and accessories.

Figure 3.2 shows the back-panel of the device. Symbol A marks the on and off switch, B is the socket for the power cable, C is the port for attaching pedals, D is used to connect EBI™ (empty bag indicator), E is for the ENDO H® (specially designed irrigation fluid heater used to prevent hypothermia) and F is the programming interface used by engineers to update the software of preform maintenance on the device.

Main function of ENDO P® is to control the pressure and the flow delivered to the operating cavity. Flow is directly controlled by setting the pump rotation speeds which is in case of peristaltic pumps related to the volumetric flow. The fluid enters the system from the fluid bags hanging on the stand that can be complemented with the EBI™ (empty bag indicator that allows the ENDO P® to monitor the fluid levels and warn the nurse and the surgeon if the bags need replacing) through the Day cassette. On figure 3.1 this tubing port on the Day cassette is marked with the light blue arrow. Fluid is then taken by the inflow pump and returned to the Day cassette with the desired flow rate. Fluid than passes through the two ports marked with the orange arrows in the figure 3.1 which allow for the ENDO H® fluid heater to be connected to the system. Such heater heats up the irrigation fluid to the body temperature, preventing hypothermia and enabling faster recovery for the patient. And finally fluid exits the Day cassette through the port marked with the red arrow and enters the tubing leading to the operating cavity. Other than being the interface for connecting different elements of the system, Day cassette also plays and important function of steadying the flow which is pulsating at the pump output but should be steady at the entrance to the tubing. The tubing on the inflow side

has a check valve to prevent the migration of the blood and debris towards the input side of the device.

After fluid goes through the operating cavity it is evacuated together with the blood and tissue through the Patient cassette and the outflow pump. In the figure 3.1 port that links the cavity with the Patient cassette is marked with the red arrow while the port leading from the Patient cassette to the waste container is marked with the blue arrow. The flow delivered to the operating cavity is approximately the same as the one at the entrance to the tubing because water is incompressible and the tubing expansion in diameter with the rise in pressure is negligible. The same statement holds for the outflow, so the flow control is easily achieved either by increasing or decreasing pump rotation speeds. This system also makes it easy to check the amount of absorbed fluid and notify the surgeon by displaying it on the screen. Set-point for the flow is predetermined by the procedure type but during the procedure, surgeon can temporarily increase or decrease it using the pedals and improve visibility without dangerous pressure increase.

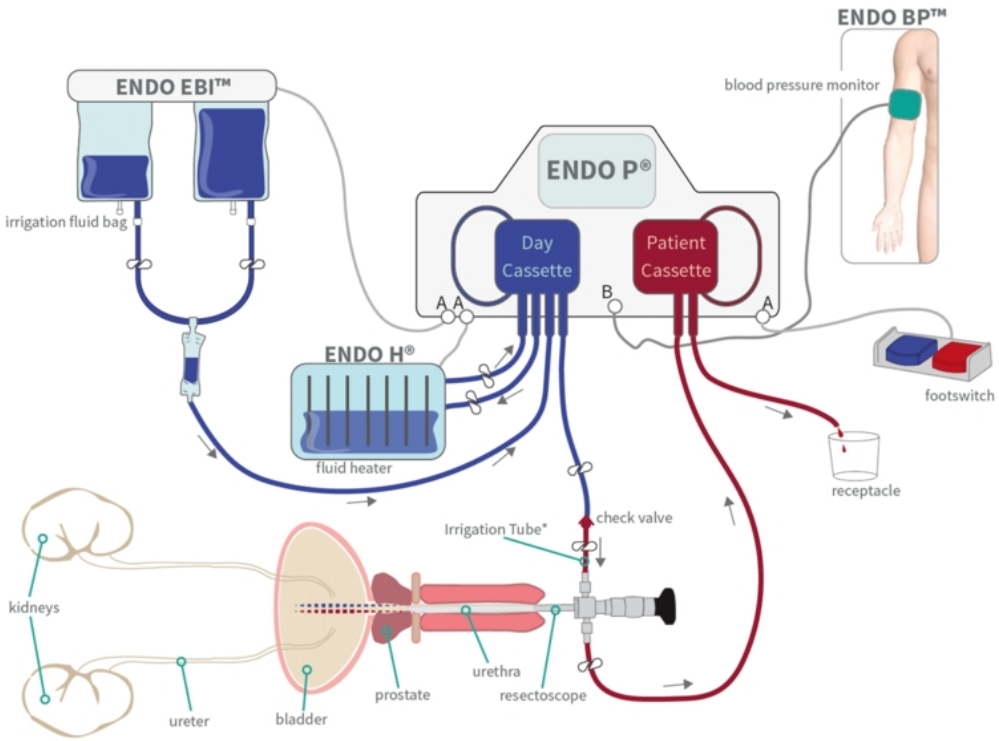

Source: http://www.bonvisi.com/products/endop.html

Figure 3.3: ENDO Pump™ System

Pressure control is a more challenging task. Monitoring pressure by inserting a sensor inside the operating cavity is impossible due to the limited space for the instrument, so the pressure sensors are placed on the ENDO P® body at the entrance to the tubing. In the figure 3.1 the pressure sensors are marked with blue circles. Two sensors are added at the input side to increase the reliability of the measurement. To correctly estimate the pressure in the cavity hydrostatic pressure and hydrodynamic pressure need to be taken into account. At the beginning of the procedure the height

difference between the patient and the ENDO P® is inputted through the graphical user interface of the touchscreen and the pressure drop in the tubing is calculated on-line based on system information. The pressure set-point maintained is derived form the blood pressure measurement preformed by the blood pressure monitor cuff connected to the system, and the control is based on the relation between the cavity volume and the pressure. Pressure set-point can also be adjusted by actuating the pedals helping the surgeon to spot and prevent bleeding by cauterizing the damaged tissue. The information regarding pressure, flow, set-points, blood pressure and fluid uptake is displayed on the ENDO P® screen. Schematic of the system with all the connected accessories can be seen on figure 3.3.

3.2 Mathematical model

ENDO P® controls the pressure in the cavity $p_c(t)$ by adjusting the pumps rotation speeds which are linked to inflow $q_i(t)$ and outflow $q_o(t)$. Some simplifications of the original system are necessary for model construction. The cassettes are assumed to convert the irregular pump flow into the steady flow instantly and the inflow $q_i(t)$ and outflow $q_o(t)$ further considered are the steady flows assumed to be delivered by pumps at the tubing entrance. Since irrigation fluid is modeled as incompressible fluid, and tubing is assumed not to increase in diameter with the increase in pressure, the flows at the entrance of operating cavity $q_{ic}(t)$ and $q_{oc}(t)$ should be the same as the flow delivered by the pumps at the entrance of the tubing, only delayed by dynamics that explain the fluid propagation through the tubing $q_{ic}(t) = q_i(t - \tau)$ and $q_{oc}(t) = q_o(t - \tau)$. Furthermore, since the flows are considered steady, and the dynamics fast compared to the rest of the system dynamics, simplified relations are derived $q_{ic}(t) = q_i(t)$ and $q_{oc}(t) = q_o(t)$. These flows constitute the input to the system.

$$u_1(t) = q_i(t)$$
$$u_2(t) = q_o(t)$$

Since the variable of interest for control purposes is the pressure within the operating cavity $p_c(t)$, mechanics of a human bladder need to be investigated. For the simplified model it is the easiest to imagine the bladder as an inflatable balloon. The pressure in the balloon grows as its elastic membrane expands to contain the volume of water that is pumped in. This elastic membrane counters the expansion of the balloon compressing the fluid inside. As the volume of the fluid inside the balloon decrease, membrane loosens and pressure decreases. So pressure is connected to the volume inside the bladder through the nonlinear relation called compliance C representing the effect of the elastic membrane or the bladder walls. In terms of the model that means that the output of the system $z(t) = p_c(t)$ is dependent on the system state, namely the volume of the fluid inside the bladder $x(t) = V(t)$. The volume can be obtained by considering the difference of the volumetric flows that

represent the inputs to the system.

$$\frac{dV(t)}{dt} = q_i(t) - q_o(t)$$

Therefore the state of the system can be expressed in the following form.

$$\boldsymbol{u}(t) = \begin{bmatrix} u_1(t) \\ u_2(t) \end{bmatrix} \tag{3.1}$$

$$\dot{x}(t) = \begin{bmatrix} 1 & -1 \end{bmatrix} \boldsymbol{u}(t) \tag{3.2}$$

Compliance is defined as the change in volume with respect to change in pressure or $C = dV/dp$. Since cavity pressure is of interest as an output it can be written $dp_c(t) = dV(t)/C$ and final output notation is reached.

$$z(t) = \int \frac{1}{C} dx(t) \tag{3.3}$$

At this point problem becomes obvious. If compliance C was just a constant the solution would be $p_c = V/C$ or simply $z(t) = \frac{1}{C}x(t)$ making this system a simple integrator. But compliance in a biological system is a function of quite a large number of different parameters, current volume of the bladder being just one of them. Patient age, fitness, maximum bladder volume, current bladder volume, muscle fatigue, procedure duration, muscle contraction (for example coughing) all influence this function making it impossible to correctly identify for each specific patient and procedure. What can be done instead is to find the maximum and minimum value and ascertain the range of possible compliance values, thus continuing with the uncertain (but limited range) integrator model of the system. For this to be done tests on the patients need to be carried out, state, inputs and the outputs of the system logged and the model verified and augmented with the new information. This further development would allow for larger variety of control strategies to be considered and compared.

Model presented in equations (3.1) to (3.3) is still incomplete. Since the ENDO P® system features pressure sensors, additional information about the output is available. Output is measured indirectly but the influence of the specific parts of the system can be estimated with good precision, thus giving the reliable value for the control purposes.

As can be seen form figure 3.4 measured pressure p_{mi} or p_{mo} is composed of three main components: cavity pressure p_c, pressure drop in the tubing Δp_{ti} or Δp_{to} and hydrostatic pressure due to height difference Δh between the device and the patient. For the pressure measured on the inflow side $y(t) = p_{mi}(t)$ following relation holds.

$$p_{mi}(t) = p_c(t) + \Delta p_{ti} + \rho g \Delta h$$

Where ρ is the fluid density and g is the gravitational acceleration. Similar equation holds for the outflow side, just the sign of the function Δp_{to} describing the pressure

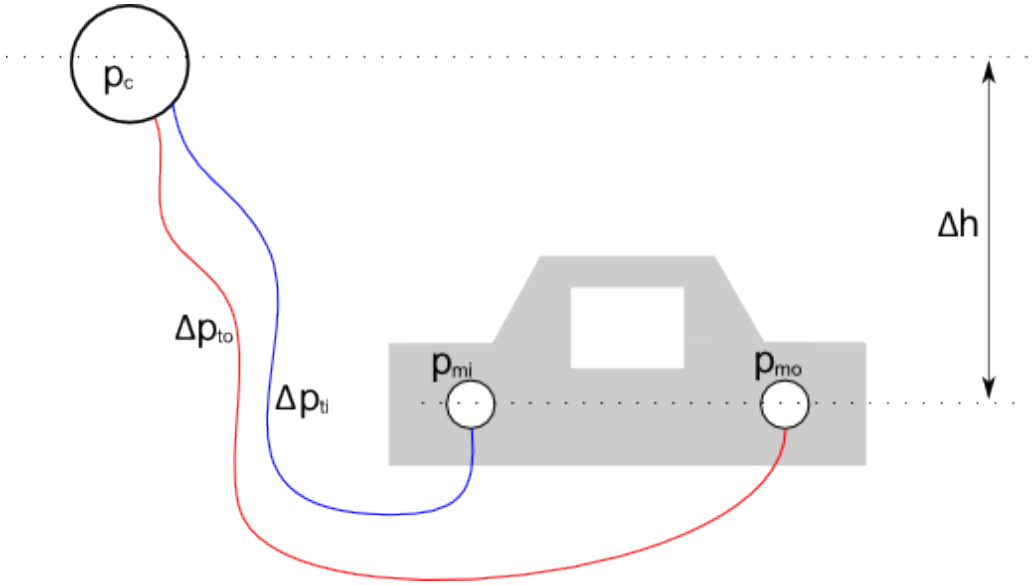

Figure 3.4: Pressure drop diagram. p_c marks the cavity pressure, Δp_{ti} and Δp_{to} are dynamic pressure drops in the tubing and p_{mi} and p_{mo} are pressures measured at sensors. Δh is the difference in height between the cavity and the device affecting the hydrostatic pressure.

drop in the outflow tubing is negative. So to complete the system representation measured pressure is also included in the description.

$$y(t) = z(t) + p_d(t) + p_{hs} \tag{3.4}$$

Where $p_d(t) = \Delta p_{ti}$ represents the dynamic pressure drop in the tubing dependent on flow, time, tubing elements and geometry, and $p_{hs} = \rho g \Delta h$ is the constant describing the hydrostatic pressure drop. Equations (3.1) to (3.4) complete the model of the system in its most condensed form.

3.3 Subsystems

The model presented in chapter 3.2 is a good starting point for the overall understanding of the system, but several things were left unanswered. How to model the functions of compliance C or the dynamic pressure drop in the tubing $p_d(t)$, and how does the ENDO P® behave in reality, more precisely how do the different subsystems influence the behaviour and interact with each other. In the following chapters 3.3.1 to 3.3.4 these questions are explored further.

3.3.1 Pumps

Peristaltic pumps are active elements in the system. Run by stepper motors they deliver wanted volumetric flow to and from the cassettes. This type of pumps use a roller to clamp the flexible tubing, thereby displacing the liquid in the direction of the roller movement. Figure 3.5 illustrates this principle.

The big advantage of this type of pumps is the separation of the pumping mechanism from the tubing that holds the liquid, making it useful in medical applications where the tubing needs to be sterile not to contaminate the irrigation fluid, like in the endoscopy pump.

Main disadvantage is imprecision. Due to flexible tubing and different clamping positions the volume delivered varies from setup to setup. Another problem is tubing deterioration so it is not uncommon that with the same rotation speed pump delivers different volumes in different points in time. The tubing is not always perfectly clamped so the pressure in the system also influences the volume. Namely due to higher pressure on the output side the inflow pump and the pockets between clamped tubing the inflow pump delivers less volume as the pressure increases and the opposite holds true for the outflow pump. One more disadvantage is the pulsating flow this kind of pumps deliver.

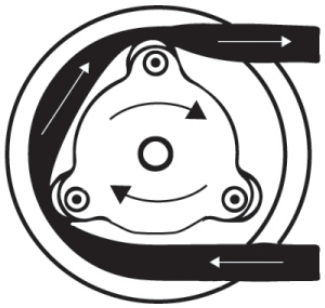

Source: http://www.pmdcorp.com/news/articles/html/precision_fluid_handling_deep_dive.html

Figure 3.5: Peristaltic pump with three rollers. As the central part rotates, rollers compress the clamped tubing pushing the liquid in the direction of rotation.

In the model so far, pump influence was not taken into account and flow was considered to be a system input. In reality, the pump rotation speeds are true inputs and volumetric flow is calculated from the identified linear function. The approximate volumetric flow could be calculated from a simple relation.

$$q_{pi} = r_t^2 \pi L \omega$$

Where the volumetric flow q_{pi} is dependent on the tubing radius r_t, L length of the tubing clamped in one rotation and ω pump rotation speed. More accurate relations

include the number of rollers, fluid models and different tubing deformation calculations. These relations will not be included in the model because the additional complexity introduced would not be justified by the benefits of additional information, since the difference from the simple model is less than the model uncertainty. Another thing worth considering for the model is that the pump is not an ideal element and it has a response time that slow enough to be included in the system dynamics.

Figure 3.6 shows the Simulink® model of the inflow pump subsystem. Pump dynamics are modeled by first order transfer function A_d with the uncertain parameter p.

$$A_d = \frac{p}{s+p}$$

The pump rotation speed was not considered and the input remained the volumetric flow. Such decision was due to the fact that rotation speed would not introduce better precision but would just represent a less intuitive input, especially considering another system set-point is flow. Pumps inherent imprecision was modeled as input disturbance partially dependent on the inflow, and the additional disturbance was added at the output of the pump dynamics to model the system pressure influence. In case of inflow pump the delivered flow is decreased as the pressure in the cavity grows.

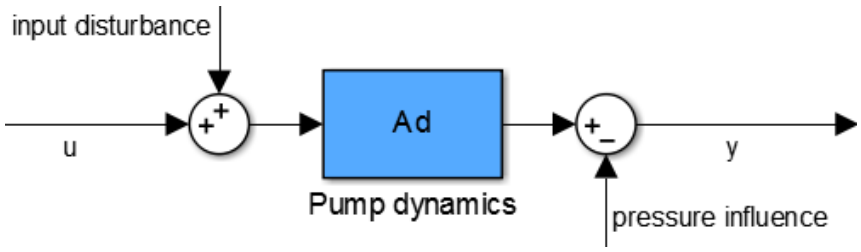

Figure 3.6: Inflow pump model. Input disturbance models the uncertainty connected with pump model identification. Pressure influence models the overall system pressure influence on the delivered flow. Both input u and output y of the subsystem are flows [ml/min].

3.3.2 Sensors

ENDO P® system features three pressure sensors located on the body of the device. Special elastic membrane is built in the Day and Patient cassettes close to the entrance to the tubing. It deforms as the pressure inside the cavity and the tubing rise and actuates the pressure sensors. Two pressure sensors on the input side monitor the pressure in the system and a pressure sensor on the output side is used to detect blockage in outflow tubing.

Pressure sensors are very precise and fast so their dynamics in the overall system is negligible. There are two interesting effects to model connected to the sensors. One is standard sensor noise and the other is the effect of the pumps. Since the flow form the peristaltic pumps is pulsating, sudden increase in volume in the cassettes affects the pressure and as the volume passes through the cassette and the flow equalizes, the pressure drops. This effect is connected to pump rotation speed and the number of rollers. This dynamics is also high frequency but, as it was observed from the initial tests, has a significant influence in terms of gain.

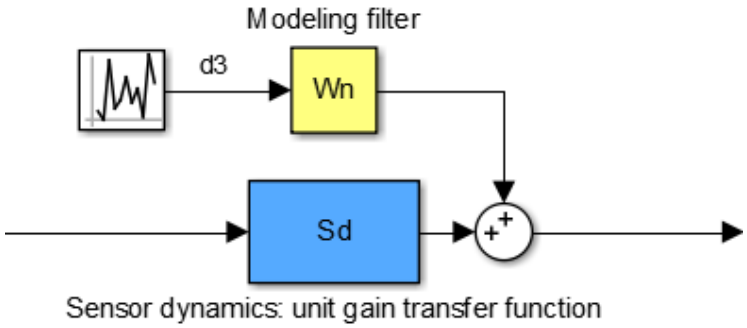

Figure 3.7: Sensor model. At the output of the sensor dynamics block the colored noise is added to simulate the disturbances. Both input and output of the sensor model subsystem are pressures [mmHg].

The model chosen for the sensors is unit gain transfer function with added output disturbance. This disturbance is normalized white noise passed through the high-pass filter that aims to model the dynamics amplifying the output. Simulink® model is shown on the figure 3.7

3.3.3 Tubing

The main interest in this chapter is to try to quantify the pressure drop in the tubing. It is essential that this relation is identified as precisely as possible, because the knowledge about the output is dependent on it. If (3.4) is rearranged this becomes obvious.

$$z(t) = y(t) - p_d(t) - p_{hs} \tag{3.5}$$

Since $y(t)$ is measured output and p_{hs} is a constant calculated in the beginning of the procedure from user input about the height difference, the key to calculating the pressure in the cavity $z(t)$ becomes identifying the pressure drop in the tubing function $p_d(t)$.

From the fluid dynamics the first relation that comes to mind is using Bernoulli equation. If friction losses are neglected and no energy is added to, or taken from a piping system, the sum of the hydrostatic, absolute and dynamic pressure related to flow velocity will be constant for any point of fluid streamline. But a simple relation

disregarding the frictional loss in this case is insufficient and the equation becomes; for two points in the streamline, $i = 1, 2$ each with its own absolute p_i, hydrostatic $\rho g h_i$, and hydrodynamic $\frac{\rho v_i^2}{2}$ pressure following holds.

$$\rho g h_1 + \frac{\rho v_1^2}{2} + p_1 = \rho g h_2 + \frac{\rho v_2^2}{2} + p_2 + p_L \tag{3.6}$$

Where p_L is pressure loss due to friction in the tubing.

Since the hydrostatic pressure in (3.5) is already taken into account and velocity, that is directly connected to flow, is assumed to be the same at the entrance and at the end of the tubing, from (3.6) only the pressure loss due to friction becomes relevant.

$$p_d(t) = p_1 - p_2 = p_L$$

Pressure loss p_L is given by Darcy's formula (3.7) which is applicable for constant tube diameter, constant fluid density and relatively straight tube.

$$p_L = \frac{\rho f L v^2}{2D} \tag{3.7}$$

Where ρ is fluid density, v is the mean fluid velocity calculated from the flow q together with the tube cross section area with diameter D,

$$v = \frac{4q}{D^2 \pi}$$

L is the length of the tubing and f is the friction coefficient.

For laminar flow regime friction factor can be calculated, but for turbulent flow regime knowledge of the pipe roughness with the experimentally obtained results for different Reynolds numbers called the Moody diagram need to be used. Between the two flow regimes, transient flow occurs making it impossible to differentiate between laminar and turbulent flow so friction factor is indeterminate, bounded by lower limit for laminar flow, and upper limit based on turbulent flow conditions.

Laminar flow regime is common for small fluid velocities when streamlines are straight and parallel to the tubing walls. Turbulent flow regime has randomly dispersed streamlines throughout the tubing and usually occurs at higher fluid velocities. An easy way to estimate the flow regime is by calculating the Reynolds number. If it is less than 2300 laminar flow regime is present and if it is higher than 4000 the flow is turbulent. For values in between it cannot be decided since the change between the flow regimes is unpredictable. Reynolds number is calculated from the following formula.

$$Re = \frac{\rho v D}{\mu}$$

Where ρ is fluid density, v is the mean fluid velocity, D tube cross section area diameter and μ fluid dynamic viscosity.

In the surgery conditions, lower flow rates are preferred as a means of reducing irrigation fluid consumption and increasing safety. No flows higher than 350 ml/min are expected. In such case, calculated flow regime is always laminar making it possible to find the friction coefficient, the last unknown in the tubing pressure drop formula.

$$f = \frac{64}{Re}$$

When all the formulae are put back together in (3.7) and simplified, the pressure drop takes on the following form.

$$p_L = \frac{128 L \mu}{D^4 \pi} q \tag{3.8}$$

Problem with this equation is that it assumes a relatively straight tube, which is in case of flexible medical tubing unrealistic. One of the possible approaches to such a problem would be to model these additional friction losses that occur in the tubing bends through extending the pipe length till the equivalent pressure drop is reached. Since tubing could move and the geometry might change during the surgery this length extension becomes an uncertain parameter. Pressure drop obtained in this systematic way is a good starting point for tubing identification because it gives the intuition about the system, but other than that it is highly impractical.

Flexible tubing that is likely to move during the course of surgery is just one of the model discrepancies. Additional elements such as check valve and endoscope all affect the flow regime and pressure drops in a rather unpredictable way. System identification carried on a test site is of more value for the final calculation.

Test site was set up using the ENDO P® with tubing connected to the endoscope and inserted into a bottle. Bottle was closed and prevented from leaking pressure. Two sphygmomanometer pressure gauges were connected to the entrance to the tubing and the bottle representing the cavity. Pumps were run at different flows from 50 ml/min to 400 ml/min and after a stable pressure in the cavity was reached, data was collected.

What was noticed from the tests results on the real system is that the relation (3.8) was right about the linear dependence on the volumetric flow, but also significantly underestimated the pressure drop. This was expected considering the additional system elements, such as endoscope and the check valve, that were not modeled in the above formulae. The results at the flow rates higher than 350 ml/min were deviating slightly from the linear relation what could be attributed to transitional zone between the flow regimes. There was also an identifiable static pressure drop whose effect is again attributed to the endoscope and the check valve.

Both the calculations and the identification carried out addressed only the static model of the system. Flow propagation through the tubing and the problematic dynamics of tubing movements were left out of consideration.

One of the reasons to exclude tubing movements is the high frequency of such phenomena resulting in system recognising them as measurement noise. Problematic part of that approach is in the fact that the pressure spikes occur in the operating cavity as well as on the sensors which could present a potentially dangerous situation for the patient. But due to the slow dynamics of the overall system, even if correctly predicted, such spikes could not be prevented. What is implemented instead is the safety mechanism that tracks overpressure and shuts down the pumps in case of dangerous overshoot. Another thing that works in favour of the this choice is that such situations are rare, and drastic tubing movements are not common in the operating room, and that spikes are very quick meaning that the exposure to increased pressure is less than a second. Since organ damage and fluid intake rely on the long term exposure to high pressure, such rare and quick spikes can be considered harmless.

Flow propagation through the tubing is another matter. While it would certainly be desirable to model this particular dynamics, due to the unknown geometry it is practically impossible. Simple delay as suggested in the chapter 3.2 could be a good guess, but the approach of adding an uncertain dynamics to the static system model could prove to be more beneficial for the control purposes, so in the Simulink® model on figure 3.8, this was chosen as a solution.

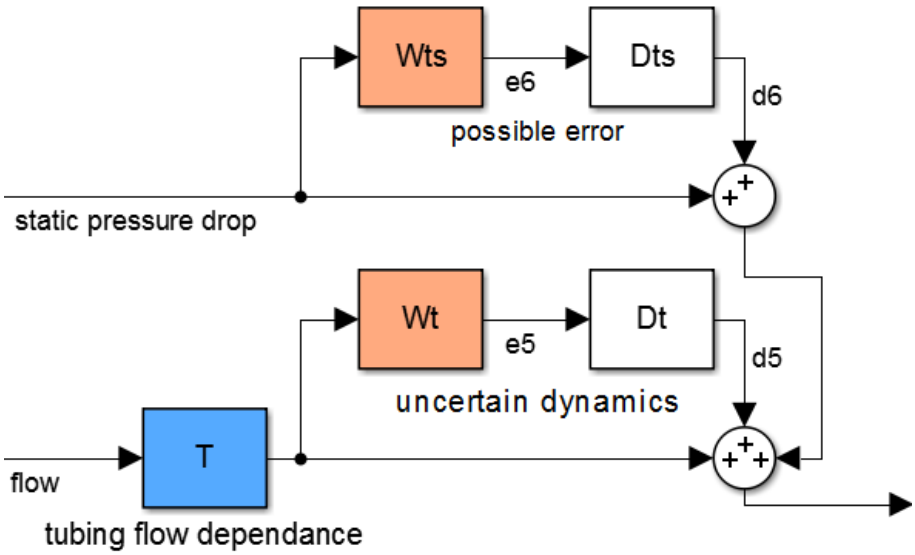

Figure 3.8: Tubing model. Static pressure drop and uncertainty model the height difference influence and the transfer function T and uncertain dynamics model the flow dependent dynamic pressure drop. Inputs to the tubing model are static pressure drop [mmHg] and flow [ml/min]. The output of the tubing model is pressure [mmHg] added to the bladder pressure to compensate for pressure drops in the tubing.

Another multiplicative uncertainty added in the model is the one connected to the static pressure drop input. The reason for this is the possible error in measuring

height difference between the sensors and the operating cavity for the hydrostatic pressure calculation and small model discrepancies that were present in the system identification tests.

3.3.4 Bladder

Modeling the human bladder which is in fact the surgical cavity is by far the most challenging part of the model. Chapter 3.2 introduced the problem and linked it to the compliance function. Compliance is dependent on a number of biological parameters like age, fitness level, bladder volume, maximum bladder volume, muscle fatigue, but also the procedure conditions and progress, like tissue damage, temporary muscle contractions and duration of the surgery. As suggested earlier, the best way to gain insight into this function would be to analyze experimental data from the surgeries to find the bounds on the function values and to better understand the dynamics of the bladder tissue. Unfortunately, collecting such data was so far impossible. With the development of ENDO P® this could be a future possibility because ENDO P® can track volume and the pressure in the operating cavity, but for now, this thesis will try to find a workaround for this problem.

3.3.4.1 Pressure–stretch curves

When considering alternatives for modeling the bladder one of the ideas is to envision it as an inflatable rubber balloon that maintains its spherical symmetry as it inflates. In modern theory of non-linear elasticity such problem is already solved. Some of these solutions offer good basis for modeling soft biological tissues such as veinous and arterial aneurysms and may prove useful when applied to the bladder modeling. This chapter will heavily relay on the paper by Destrade and Mangan [6] *Gent models for the inflation of spherical balloons* and will analyze and reproduce some of their results and figures in a attempt to better understand the bladder tissue model. Of specific interest will be their results fitting the 3-parameter phenomenological model of hyperelasticity to the experimentally obtained monkey bladder data.

Consider a spherical shell made of an incompressible isotropic hyperelastic material, deforming by inflation and maintaining spherical symmetry, with the initial inner radius A and outer radius B, and with inflated inner radius a and outer radius b. The thickness parameter of the shell is defined as $\delta = (B - A)/A$ and the stretch is given by the following relation.

$$\lambda = \frac{a}{A}[1 + \mathcal{O}(\delta)] \tag{3.9}$$

Pressure-stretch relation as derived in Destrade and Mangan links the excess of internal pressure P with the $\hat{W}$, the auxiliary function connected to strain energy

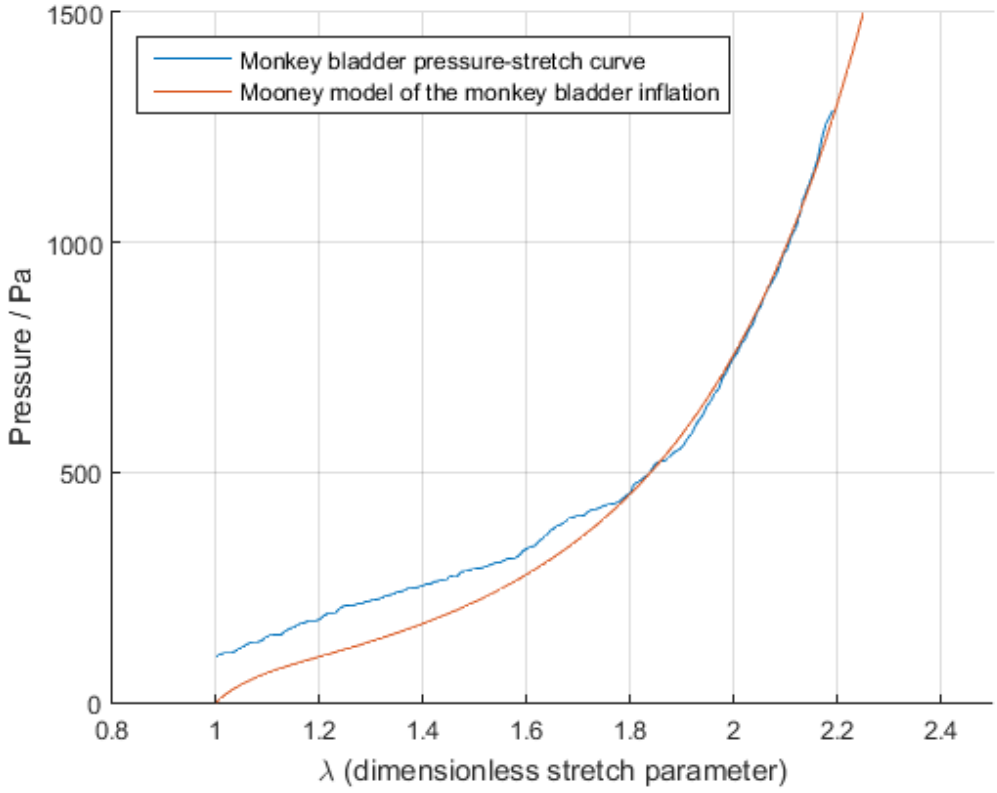

Figure 3.9: Monkey bladder pressure-stretch curve. Blue curve is the monkey bladder data adapted from Osborne and the red curve is the fitted Mooney model with parameters: $C_1 = 31.75$, $C_2 = 0.28$, $n = 6.05$.

density function.

$$P = \delta \frac{\hat{W}'(\lambda)}{\lambda^2} \tag{3.10}$$

By choosing a constitutive model through energy density function, relation (3.10) can be used to plot the pressure–stretch curves for a thin shell subject to inflation. One of the 3-parameter phenomenological models of hyperelasticity proposed by Mooney [7] gives expression for the strain energy density function.

$$W_M = C_1(\lambda_1^n + \lambda_2^n + \lambda_3^n - 3) + C_2(\lambda_1^n\lambda_2^n + \lambda_2^n\lambda_3^n + \lambda_3^n\lambda_1^n - 3)$$

Where $C_1, C_2, n > 0$ are model parameters and λ_1, λ_2 and λ_3 are principal stretches which represent radial stretch λ_1 and circumferential stretch λ_2, λ_3 in case of the spherical elastic shell. Putting the W_M into the relation (3.10) gives the equation used to find curves explaining the expansion of the monkey bladder.

$$P = 2n\delta[C_1(\lambda^{n-3} - \lambda^{-2n-3}) + C_2(\lambda^{2n-3} - \lambda^{-n-3})] \tag{3.11}$$

Data for monkey bladder expansion used by Destrade and Mangan was taken from Osborne [8]. Initial radius of the monkey bladder is given as 1.3347 cm and the

thickness was taken to be 2 mm so that $\delta \simeq 0.15$. The curve with parameters $C_1 = 31.75$, $C_2 = 0.28$ and $n = 6.05$ provided the best fit in terms of minimal square error in the region of stretch $\lambda \in [1.7, 2.19]$. Figure 3.9 shows the data for the monkey bladder together with the Mooney model fitted to it.

3.3.4.2 Simple nonlinear model

The model of the monkey bladder inflation is a static one, expressed in terms of stretch. For the overall system model it would be better to have a pressure-volume relation and a simpler equation describing approximately the same behaviour. Another point would be generalization of the model. Model given in 3.3.4.1 is focused on just one monkey bladder and cannot be considered representative of the average human bladder. But the noticeable similarities in comparison of the dog, cat and two monkey bladders given by Osborne [8] allow a certain degree of generalization.

Stretch defined by (3.9) is dependent on the initial radius, current radius and the thickness of the shell. Considering that the thickness is small it can be neglected. The above obtained results can than be reused in terms of pressure-radius relations just by multiplying the stretch λ with the initial radius. This in terms allows for the pressure-volume relations to be used since one of the assumptions is the spherical shape with volume $V = \frac{4}{3}r^3\pi$.

Pressure-radius curve obtained in such way was fitted by the curve fitting tool in MATLAB® and a simpler power function $y = ax^b$ proved to be the best match.

According to Hole [9] maximum bladder volume is about 500 ml. Assuming the same tissue model but different maximal bladder volumes, pressure-radius relation was translated in the direction of the positive radius axis. This assumption is partly justified by the Osborne results. The resulting curves were also fitted with the power function in attempt to find the expressions for the a and b parameters that can model the bladders with different volumes. Volumes ranging from 300 ml to 700 ml were considered. Parameter b proved to be a result of an increasing linear function while a showed no such simple relation but instead specific values had to be obtained by cubic interpolation. This is best illustrated on the figure 3.10. On the horizontal axis of both graphs maximum radius increments represent the translation of the initial pressure-radius curve in the direction of the positive radius axis, zero representing the initial curve of a bladder with approximate maximum volume of 300 ml and the maximum radius increment of 1.35 representing one of the translated curves describing the bladder with approximate maximum volume of 700 ml.

Figure 3.11 shows the obtained bladder models. It is important to note that whenever the above text refers to maximum volume or maximum radius the term maximum denotes the volume or radius at a unrealistically high pressure that would probably lead to tissue damage and leakage. Term maximum is taken in a biological sense rather than mathematical one, since the power function used to model this phenomena is a monotonically increasing function.

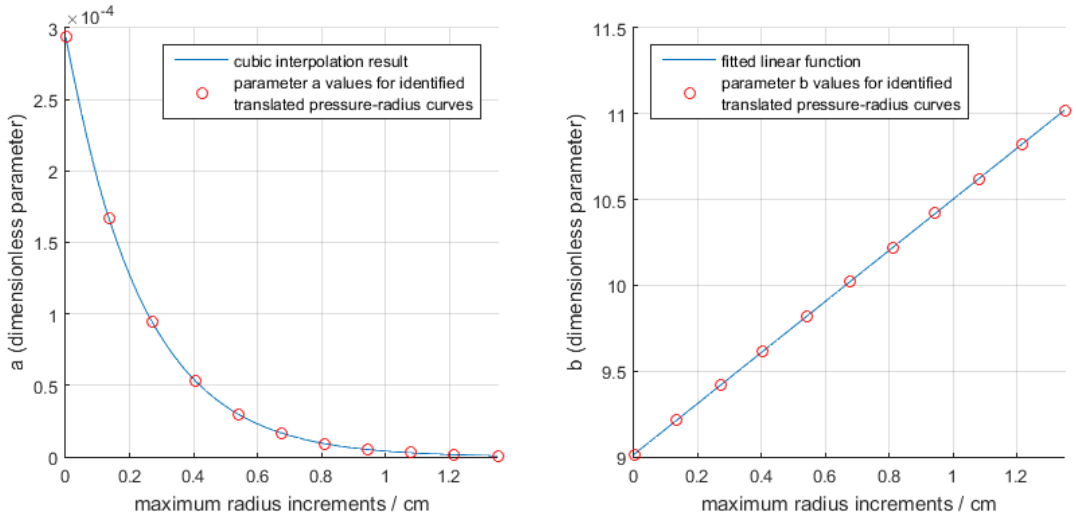

Figure 3.10: Parameters a and b of the power function. Left figure shows the parameter a trend following radius increments. Right figure shows parameter b linear dependence on radius increments. Red circles are sampled points.

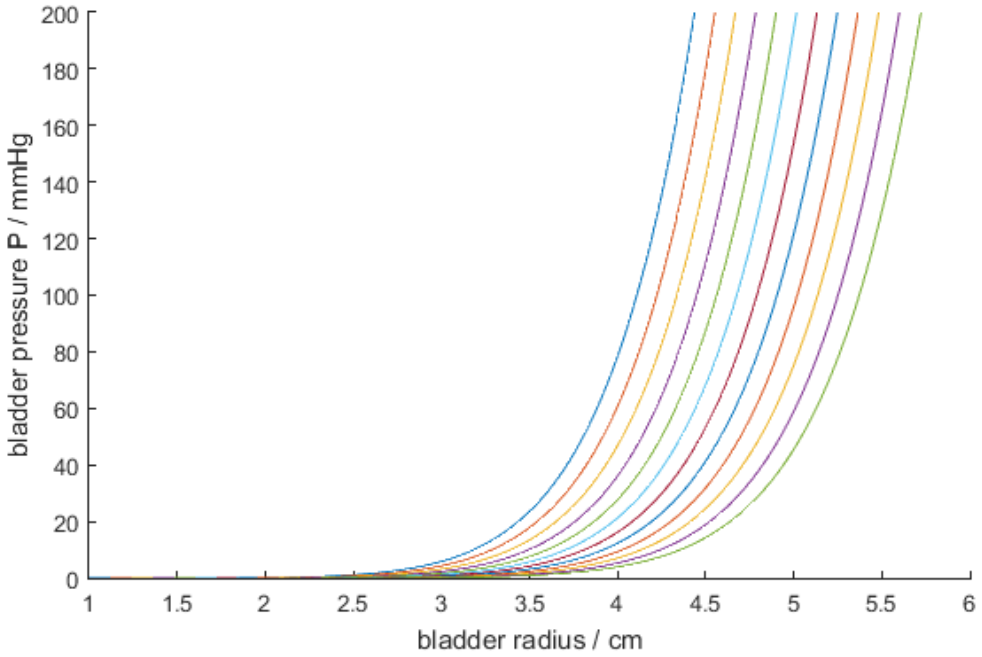

Figure 3.11: Bladder models with different radius. Each line represents a single bladder model with different maximum radius. Higher radius means larger bladder volume.

In short, a simpler bladder model was obtained by curve-fitting the power function to the complex Mooney model. To generalize the model under the assumption of different maximum radius several more bladder models were created by translating the original one along the radius axis. All of them were fitted with the power function

$y = ax^b$ and the expressions relating parameters a and b and the translation were found. That resulted in the figure 3.11 which shows a set of models for bladder with different maximal volume.

And finally the question of dynamics arises. Modeling the muscle contraction and fatigue would be ideal because, just as Osborne notes, the muscles play a predominant role in the real bladder behaviour and a model without muscle dynamics is just a bladder tissue model.

In the accurate model the muscle influence, the problem of biological parameter uncertainty arises once again. Due to complexity of this problem and relatively small gain in terms of the entire system model this thesis will consider just the simplest occurrence of pressure rise and pressure drop due to muscle contraction and relaxation.

Considering the bladder filling with fluid and muscles contracting to prevent the expansion, rise in pressure occurs. Assuming the muscles prevent full expansion, steep pressure rise occurs sooner. Once the operating pressure is reached volume is maintained by equalizing the flows.

If at some point muscles around the bladder walls tighten, like it happens in case of a cough, the pressure follows the muscle dynamics. Since muscle dynamics is unknown, a stepwise increase in pressure as the worst case dynamics is assumed. Volume of the fluid remains the same because it is controlled by the inflow and outflow and incompressible fluid assumption is imposed.

As the muscles become fatigued, pressure drops in the cavity follow the muscle relaxation. From the intuition gained in conversation with the surgeon these pressure drops are also sudden rather than gradual and are thus modeled by the stepwise drops in pressure, again with the constant volume.

In the final nonlinear model, dimension of time is added to the pressure-volume relation. As the simulation progresses, pressure-volume curves parameters a and b change causing a stepwise transition to the "lower" curves in case of pressure drop, and the opposite in case of pressure rise. This behaviour aims to loosely model the muscle influence and provide a challenge for the pressure control.

3.3.4.3 Uncertain linear model

For the purpose of control synthesis, especially in case of the robust methods, linear time invariant (LTI) model of the bladder is needed. To obtain such a model the time dependent muscle action is disregarded and the simpler pressure-radius curves derived in 3.3.4.2 are considered.

First these curves need to be translated to pressure-volume relations. Spherical shape is assumed $V = \frac{4}{3}r^3\pi$ and radius expressed as a function of volume is put into

the power functions $y = ax^b$.

$$p_c = a\left[\left(\frac{3}{4\pi}V\right)^{\frac{1}{3}}\right]^b \tag{3.12}$$

To simplify the equation (3.12) new parameters a_v and b_v are introduced.

$$a_v = a\left(\frac{3}{4\pi}\right)^{\frac{b}{3}}$$
$$b_v = \frac{b}{3}$$

And the final simplified relation is once again a power function.

$$p_c = a_v V^{b_v}$$

Linearization then proceeds in usual fashion.

$$p_{lin} = \left.\frac{dp_c}{dV}\right|_{V_0} V$$
$$p_{lin} = a_v b_v V_0^{b_v - 1} V \tag{3.13}$$

Choice of the operating point for linearization V_0 is complicated by the fact that the function needs to describe a set of curves with operating points ranging from 30 to 120 mmHg. It is clear that this parameter cannot be a single value, but on the other hand, the piecewise linearization complicates the problem further. A good trade-off in such a case is to introduce an uncertain parameter which will model all the slopes of interest for the control synthesis.

Therefore only two operating points need to be considered for V_0 which will become the bounds for the slopes modeled by uncertain parameter C_u. Tangents found at the steepest curve at the operating point pressure of approximately 130 mmHg, and volume of 320 ml, and at the least steep curve at the operating point pressure of approximately 30 mmHg, and volume of 490 ml were chosen to represent the linear model slope bounds. This specific pressure range was of interest because it is a common pressure range for the surgery conditions, where the reference is given by the percentage of the blood pressure, measured by the blood pressure monitor cuff.

Figure 3.12 shows the nonlinear pressure-volume curves and the points at which tangents are calculated together with the linear model at upper and lower bound of the uncertain parameter. The space between the light blue and dark red line represents all the interesting linear models of the relation (3.13).

Finally the linear uncertain model of the bladder is obtained.

$$p_{lin} = \frac{1}{C_u}V \tag{3.14}$$

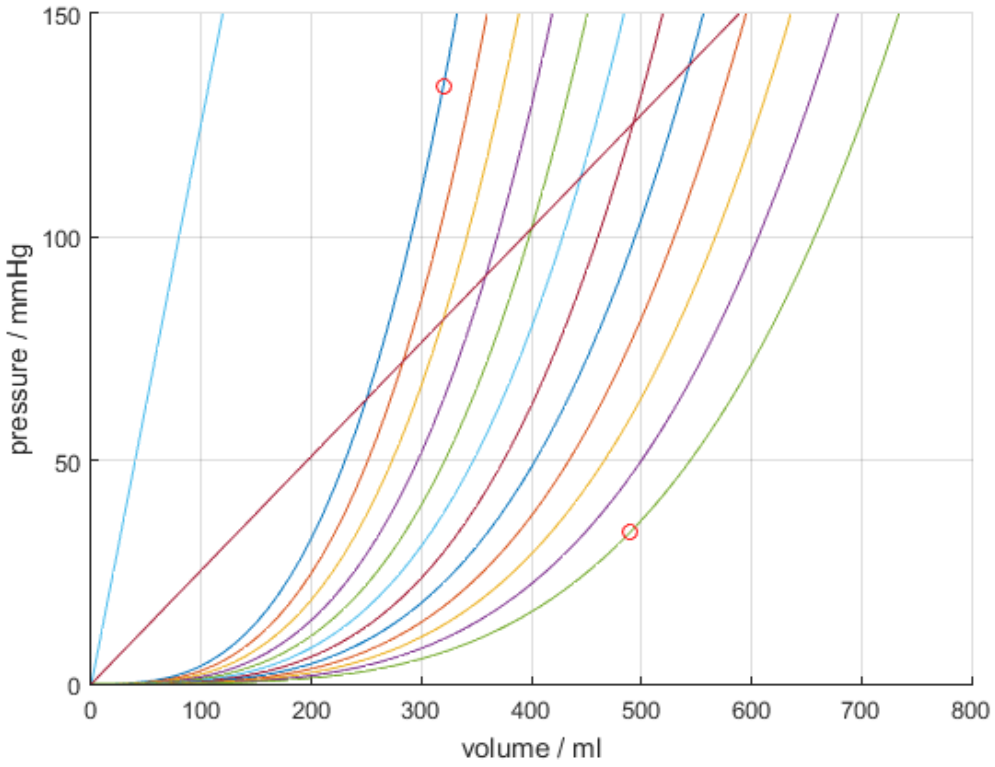

Figure 3.12: Uncertain linear model of the bladder. Considering the slopes of the nonlinear bladder models two red circles mark the chosen linearization points that produce the two linearised models that limit the uncertain state space.

Where $C_u \in [0.8, 3.9]$ is an uncertain compliance parameter. Equation (3.14) in a somewhat different form was already seen before while discussing the mathematical model in chapter 3.2 under the assumption that compliance is constant. The proposed way was to find the compliance bounds from the clinical trials with the intent of further system identification. For the time being, bounds found in this theoretical way, leaning on all the above noted assumptions will have to suffice.

To conclude the linear bladder model chapter another point needs to be raised. Uncertain linear state space as seen from the figure 3.12 does not match up so well with the nonlinear one. Higher pressures are achieved for lower volumes and the lines do not look very representative. A point could be raised that it is better to encompass the interesting part of nonlinear state space with the linear functions instead of focusing on matching the slopes. Since it was quite an easy alteration concerning only the compliance function bounds, control synthesis was done for that model as well. What was expected and eventually confirmed is that such a modeling decision leads to a more aggressive controller, which is not as robust as the one obtained with the above presented model and sometimes causes oscillations in the nonlinear uncertain system, although its overall performance can still be considered good. This is because the slopes of such linear model are lower and the controller

expects a slower reaction from the system. Another reason for the different choice of model is that for control, output feedback is going to be used and capturing the system dynamics is more important than capturing the system state space as in the case of state feedback. For all the above reasons, the presented model was chosen and the different linearization choice will not be discussed further in this thesis.

3.4 Simulink® model

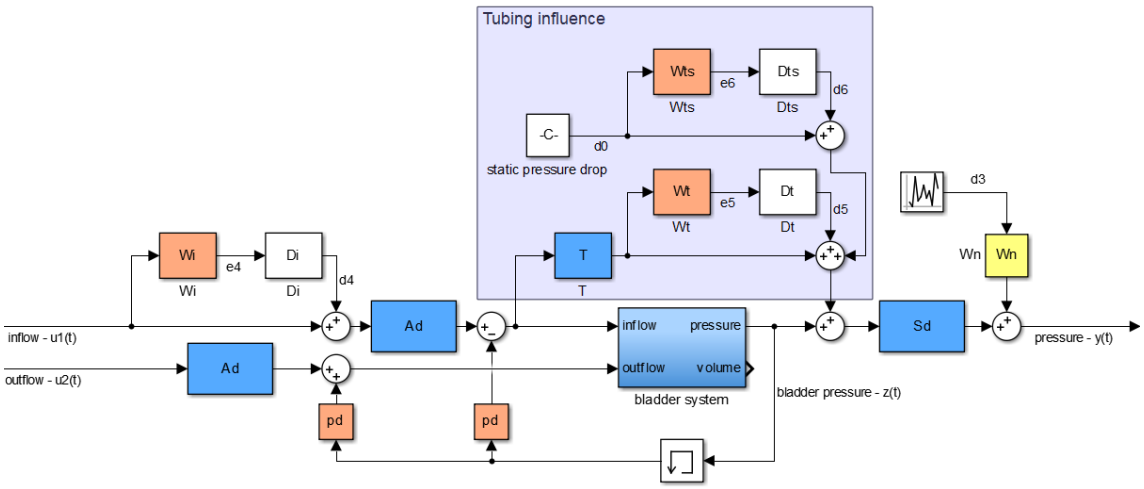

Figure 3.13: Simulink® model of the system

Figure 3.13 shows the complete Simulink® model of the system. This model will be used in chapter 4 for the purpose of control synthesis and simulation. Inside the *bladder system* subsystem linear or nonlinear model will be used depending on application. Some specifics or alterations of the original model for the purpose of control will be further explained in the coming chapters. Values of modeling filters, uncertainties and implementation specifics can be found in the MATLAB® scripts in the Appendix.

4

Control design

Before introducing control schemes and different controller structures, the question of the system output needs to be resolved. Since there is a difference between the measured output and the output representing the cavity pressure, and only the former is available in the real system, it is clear that some adjustments are needed. Reference is always given in terms of the cavity pressure, while the output is the measured pressure with the added influence of the tubing and the sensors. This kind of mismatch needs to be resolved before the error signal that goes into the controller can be calculated.

Approach taken by this thesis is to introduce a prefilter, filtering the reference and simulating the tubing influence. This prefilter is based on the tubing identification, but unlike the real tubing model, it cannot account for the model uncertainties. In this way, new reference is formed and the measured pressure can be connected in feedback. The possible problem this filter introduces is the wrong reference signal in case of uncertain tubing dynamics. These errors can be reduced by more accurate identification of the tubing, and thus the more accurate filter dynamics, but due to complex tubing geometry it can never be completely correct.

Another filter added to the measured output of the system is a simple low-pass filter. It is used to filter out the fast sensor dynamics and pumping influence, reducing the noise in the error signal.

These two filters are common for all the control strategies presented below, and both of them are designed relying on the familiarity with the system.

Simulations for each controller suggested are done on the nonlinear model of the system. The intention was to test the controller behaviour under stress, so the chosen pressure and flow references are not realistic, and would be much steadier in the real surgery conditions.

4.1 Zone bang-bang (finite state machine)

Zone bang-bang is a controller scheme based on delivering predetermined control signals depending on the magnitude of the error. Error is sorted into the zones depending on the distance from zero and constant predetermined control signals are applied depending on the active zone. Such control scheme resembles a finite state machine where zones represent the states limited by certain bounds, error variation causes transitions and control signal represents state outputs. The greatest advantage of this particular control scheme is in the fact that there is no need for an elaborate system model. It is sufficient just to have an intuition about the real system, since this particular method relies on tuning rather than optimization.

4.1.1 Theory

Since the idea behind this controller is to react based on magnitude of the error, it makes it quite similar to the simple proportional control, but unlike the proportional control, zone bang-bang consists of the look-up table with stored control values applied depending on the zone.

There are a number of tuning parameters in such controller realization. First, number of zones should be decided based on the intuition of the designer. In the simplest variant, two zones can suffice, one amplifying the control signal and the system energy and another doing the opposite. This is the idea behind simple bang-bang control. Problem in such control is obvious, crossing of border that delimits two zones gives rise to a stepwise change in control signal, and consequently introduces possible oscillations in the system output. What is often done in this case is to add a hysteresis so that the zone crossing is allowed some time, making the frequency of oscillations lower. It is important to note that such control scheme works well on systems with slow dynamics, but is far from desirable for the faster systems.

Increasing number of zones can lead to a more precise and less oscillatory control. But the more zones introduced, the more tuning parameters need to be considered. Each zone need its boundaries, which adds two additional parameters, and its control signal values, which are in the case presented again two parameters: inflow and outflow values.

Even with more zones, this control scheme often gives rise to problematic oscillations, especially if there are disturbances acting on inputs or outputs of the system, always steering the system away from the steady zone and keeping it on a boundary between the lower or the upper zone. This is something that will most likely be confirmed by the simulations, due to different disturbances modeled in the system.

In the case of zone bang-bang modeled for this study 7 zones were deemed sufficient. In zones 1, 2 and 3 the system keeps the higher inflow and the lower outflow building

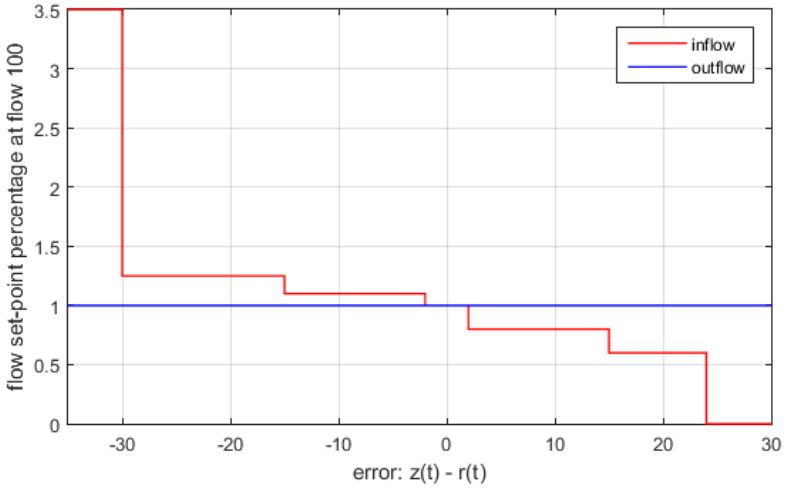

Figure 4.1: Zone bang-bang: control signal values. Outflow (blue) is kept constant and inflow (red) is varied to control pressure. Differences in flows are larger as the error is further from zero to make the effect of pressure drop or rise faster.

up pressure in the system. Zone 4 is devised as a steady zone with equal flows, and zones 5, 6 and 7 are meant to reduce pressure in the system by decreasing the inflow and increasing the outflow. Graphical interpretation of this scheme for the flow reference of 100 ml/min is on the figure 4.1. From the figure it is obvious that the zone boundaries or applied inflow control signals need not be symmetric. These values are used for tuning the controller and it makes sense to be more careful while building pressure and be somewhat faster in reducing it. The first zone where inflow is significantly higher than the outflow is modeled in such a way to speed up the initial system pressure buildup while the seventh zone stops the inflow pump completely to prevent the pressure from rising further in case of blockage. Outflow is kept constant throughout the zones. Since the difference in flow drives the system, it is enough to vary one of the flows, while other is better kept at the reference value.

4.1.2 Simulation results

All the simulations were done on a nonlinear model of the system.

Figure 4.2 shows the control signals delivered by zone bang-bang controller. Since the outflow follows the reference, it is stable, but the inflow signal is oscillatory. As mentioned earlier, if there is a disturbance in the system, it is likely that the control signal will hit the boundary and cause oscillations by crossing it. From what can be see on figure 4.2 that is exactly what happens in this case. Control signal is oscillating around the upper boundary, constantly trying to raise the pressure which seems to be dropping due to disturbance.

Figure 4.3 shows the measured pressure at the sensors and its reference given by

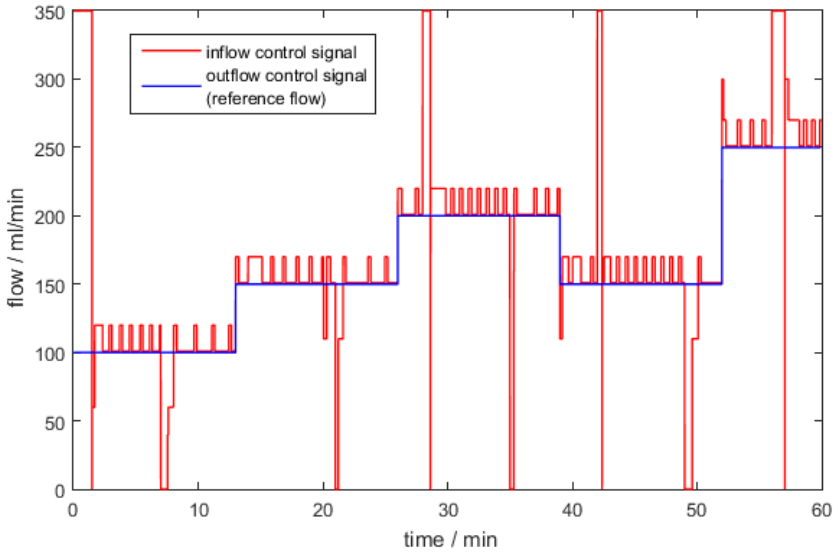

Figure 4.2: Zone bang-bang: simulated control signal values. Outflow (blue) is the reference flow and the inflow control signal (red) spikes coincide with pressure reference changes and disturbance rejection.

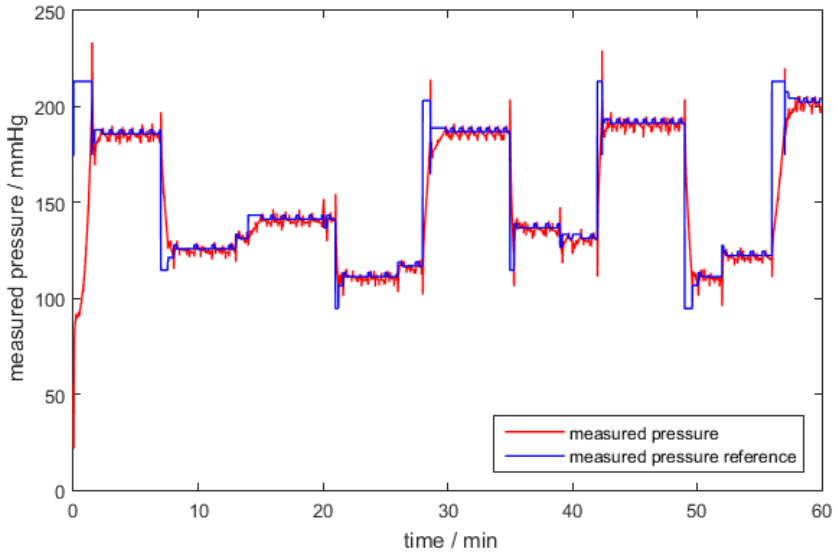

Figure 4.3: Zone bang-bang: measured pressure and reference. Measured pressure is the pressure visible on the sensors of the system consisting of the bladder pressure, pressure drop in tubing and disturbances.

the prefilter. The measured pressure is quite noisy which is the consequence of the disturbances added at the sensors.

In figure 4.4 the cavity pressure and its reference are plotted. The controller exhibits

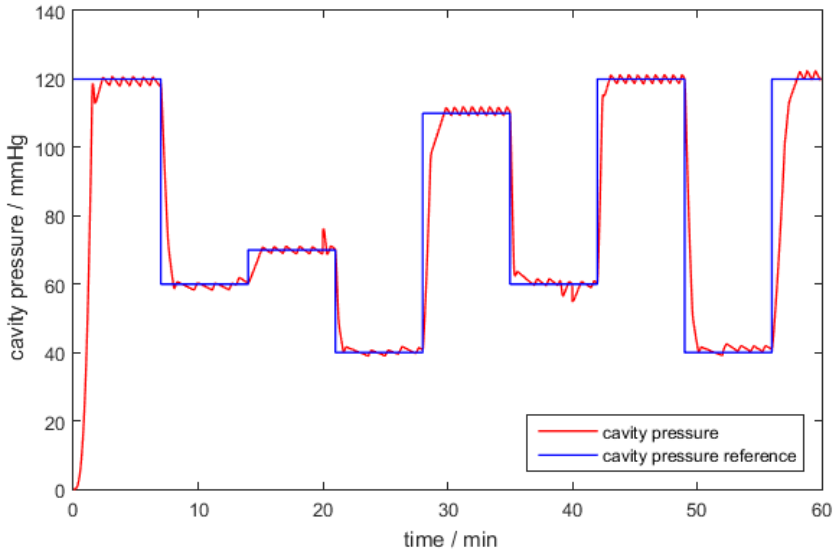

Figure 4.4: Zone bang-bang: cavity pressure and reference. Cavity pressure is not directly measured and can only be observed in the simulation environment.

good performance. The output pressure is good at following reference, it is a bit slower on the rise, but that is to be expected since it was tuned to avoid too fast pressure increase. It also shows disturbance rejection qualities, at times 20 min and 40 min disturbances in the system in form of altered compliance are added and the controller manages to correct the behaviour in reasonable time. What seems to be the issue with this controller is that the cavity pressure is oscillatory.

Figure 4.5 show a part of the system response together with the inflow control signal. From this figure it becomes clear that the oscillations in the output are due to oscillations in the control signal which is a fault of the controller.

Figure 4.6 shows how controller handles model uncertainties. Some deviation from the reference signal is expected due to highly uncertain tubing model. Prefilter cannot always correctly estimate the tubing dynamics and the pressure drop in tubing, so reference given to the controller is not precise. Despite the problematic reference signal, controller still shows a rather poor performance, with reference tracking errors up to 5 mmHg. Special cause for concern is reference tracking error displayed at flow 250 ml/min for a sudden rise in pressure. In such a case flow dependent and pressure dependent input disturbances are too large for controller to handle and errors as big as 30 mmHg can be observed. This particular situation can be fixed by making the controller also flow dependent but that can in turn result in even greater oscillations in the control signal and the system output.

Altogether, this controller shows good performance for slow systems, sufficient system disturbance rejection, a system model is not a pre-requisite and is rather simple to implement. It has a large number of tuning parameters, which can both be an

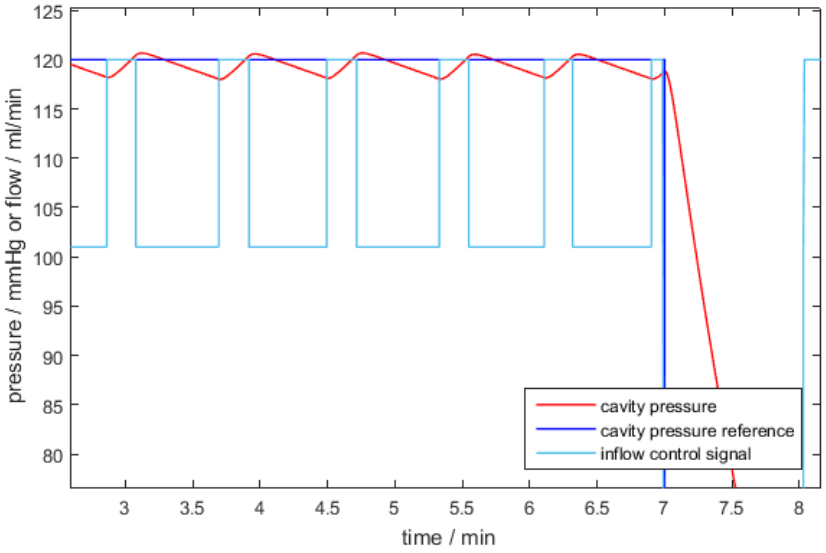

Figure 4.5: Oscillations in the cavity pressure. Magnified part of the figure 4.4 overlaid with the inflow control signal to demonstrate the effect of the unsteady inflow. Ripples in the cavity pressure match the period of those introduced by inflow.

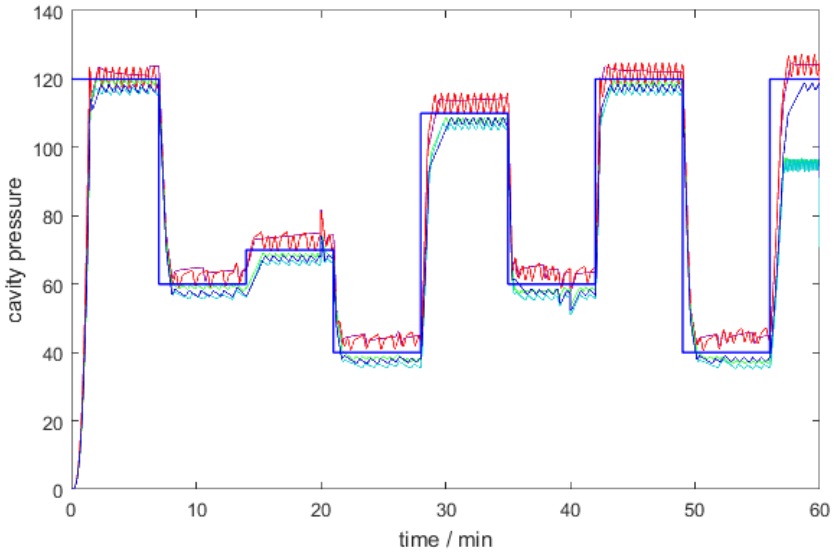

Figure 4.6: Zone bang-bang: system uncertainty influence on cavity pressure. Five different random simulations are presented.

advantage in adjusting the system behaviour but also the cause of confusion and mistakes that are not easy to trace. This particular controller causes stable oscillations and uncertainties and input disturbances greatly influence its performance. One of the biggest issues of this controller is an unsteady control input which is problematic for actuators.

4.2 PID

PID (proportional - integral - derivative) controller has for a long time been standard industry practice. Easy to implement and tune, reliable and simple, with many algorithms extending its basic functionality it is the controller of choice for both simple and more advanced system. Often it is used as a backup controller for the more sophisticated algorithms.

4.2.1 Theory

PID is an output feedback controller that consists of three terms which are added together to produce the control signal. P represents the proportional term, I is the integral term and D is the derivative one.

Proportional terms multiplies the error between the reference and the output $e(t) = r(t) - y(t)$ with the proportional gain K_p. Such term reacts to the current error value. Integral term is dependent both on the error value as well as the duration. Multiplied by the integral gain K_i the error is integrated over time to produce the output of the integral term. And finally, the derivative term acts on the rate of change of the error predicting its future values and multiplying it with the derivative gain K_d. All these terms added together make the control input to the system.

$$u(t) = K_p e(t) + K_i \int_0^t e(\tau)\,\mathrm{d}\tau + K_d \frac{\mathrm{d}}{\mathrm{d}t} e(t) \tag{4.1}$$

Since the derivative term can be too sensitive to output noise and can cause instability it is often omitted. Controller without the derivative term is called the PI controller. This thesis will further study the PID controller in its PI form omitting the derivative term due to the high amount of model uncertainty.

PI controller can, depending on the error, produce very large or unrealistic control signals. This is a problem with the actual implementation where the control signals need to be kept in the range of actuator ability. For this purpose saturation is added to the output of the PI controller. This in term leads to another problem, integrator windup. Integrator windup is an occurrence where the integral term causes overshoot due to accumulated error that produces positive controller output even after the error becomes negative. To solve the problem anti-windup method clamping is added to the controller.

Clamping or conditional integration is a scheme where integration is stopped if the saturation limits are hit and if the controller output has the same sign as the error. Figure 4.7 shows the implementation of the PI controller with anti-windup.

In the control scheme developed, outflow is kept constant at the reference value

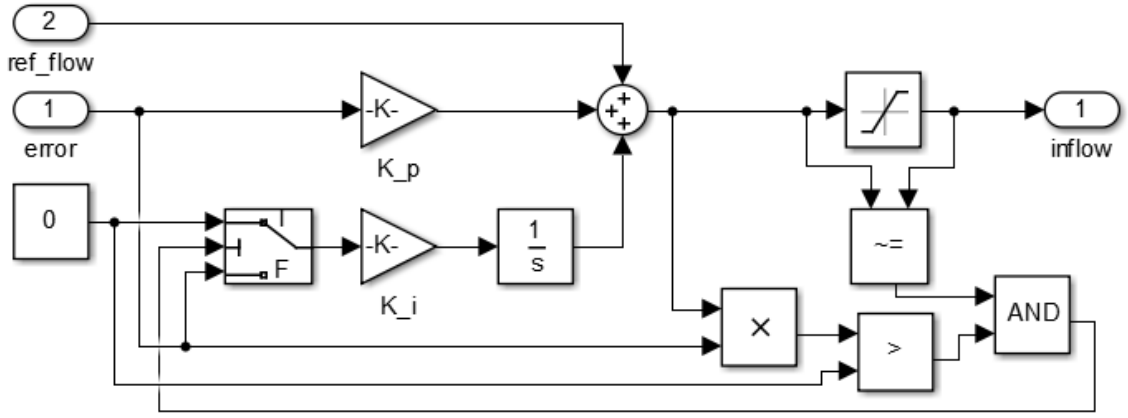

Figure 4.7: PI with anti-windup. K_p and K_i are tunable parameters of the controller. Anti-windup scheme implemented is conditional integration.

and the difference in inflow and outflow that drives the system is controlled just by varying the inflow signal. Saturation limits are placed at 350 ml/min and 50 ml/min.

4.2.2 Simulation results

Simulations were done on the nonlinear system. Tuning of the PI was preformed using MATLAB® Control System Designer tool and the linear system. First Ziegler-Nichols method was tried but resulted in far too aggressive control with unsteady control signal and oscillatory system response. Further tuning was done by MATLAB® implemented robust response algorithms and intuition. Final results are shown on the figures below.

Figure 4.8 shows the control signals. The offset the inflow has from the reference is a correction term to maintain the pressure which is otherwise leaking. The spikes in the figure are a consequence of pressure reference changes and internal disturbances like the changes in compliance at 20 min and 40 min. Other than that, the inflow control signal shows stable performance and presents quality control signal for the real actuators.

Figures 4.9 and 4.10 show the reference tracking performance of the controller. What is noticeable is the slight overshoot that happens upon reference change. This is due to integral action of the controller. System is quite stable and good at disturbance rejection. At the worst undershoot peak, i.e. at the highest flow rate and thus highest influence of uncertainty in the tubing identification, the reference tracking error for the nominal system is around 7 mmHg.

Figure 4.11 shows the performance of the system under randomly sampled uncertainty. What can be seen is consistent performance with variable offset from the

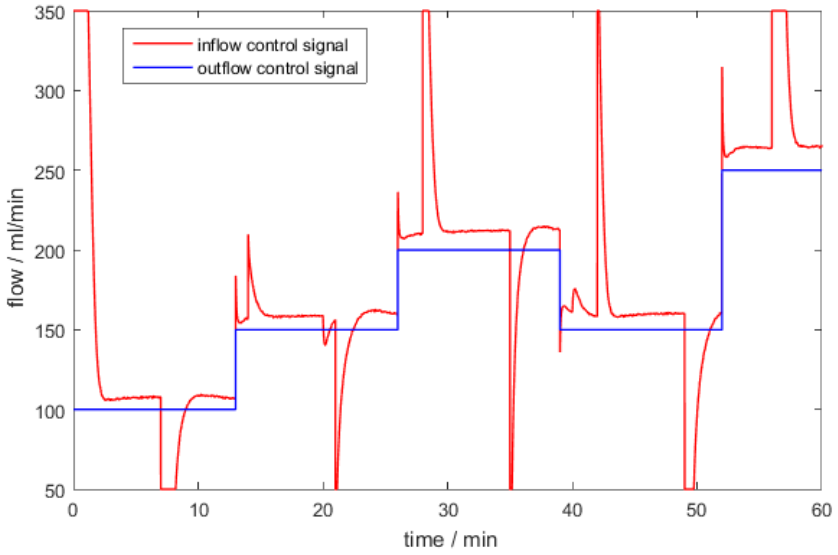

Figure 4.8: PI: control signal values. Outflow (blue) is the reference flow and the inflow control signal (red) spikes coincide with pressure and flow reference changes and disturbance rejection.

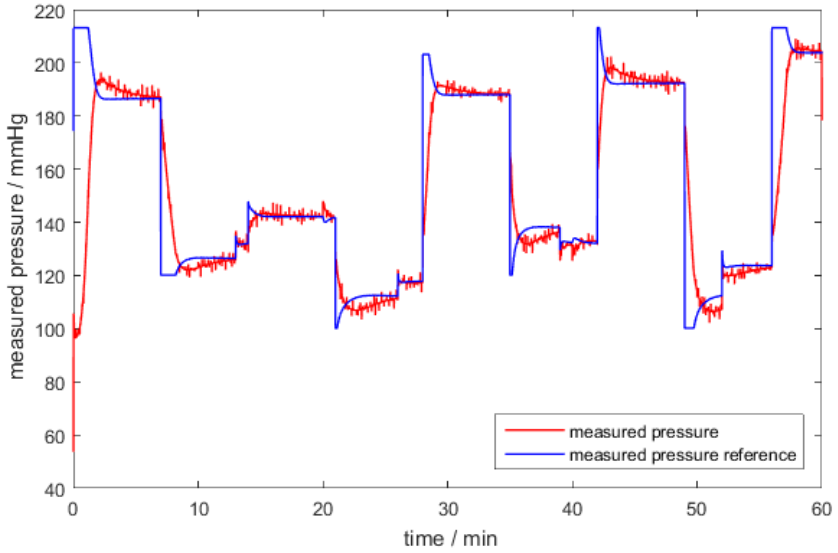

Figure 4.9: PI: measured pressure and reference. Measured pressure is the pressure visible on the sensors of the system consisting of the bladder pressure, pressure drop in tubing and disturbances.

reference for differently sampled uncertain values. These offsets range up to 10 mmHg in magnitude.

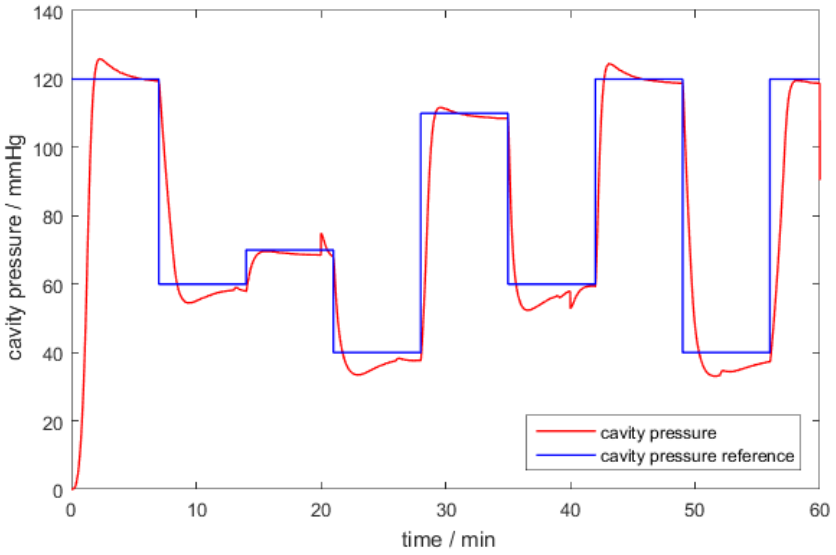

Figure 4.10: PI: cavity pressure and reference. Cavity pressure is not directly measured and can only be observed in the simulation environment. Spikes at times 20 min and 40 min are a consequence of internal disturbances of the bladder model.

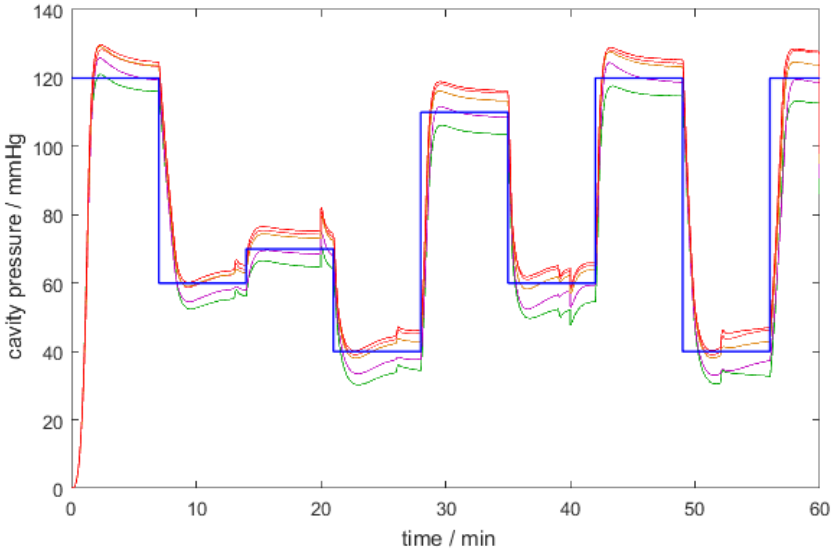

Figure 4.11: PI: system uncertainty influence on cavity pressure. Five different random simulations are presented.

4.3 $\mathcal{H}_\infty$ structured control

PID control has been the industry standard for a long time and it owes its popularity to the simplicity and ease of implementation. It is familiar and reliable, but also outdated from the perspective of modern control.

New methods and theories provide much better results in terms of response quality or system stability. Most of these methods feature heavy theory, complex optimization algorithms, that can be solved only with help of advanced software, and different structures not always useful in embedded systems applications.

But what if the familiar form of the PID control could be optimised instead of tuned? Easily implementable PID controller with the parameters chosen in the optimal way through an optimization algorithm could possibly be the solution to utilize the benefits of both control strategies.

4.3.1 Theory

This chapter aims to present the $\mathcal{H}_\infty$ control problem, hint at the structured controllers as a viable solution and give references for further reading. Nonconvex and nonsmooth optimization algorithms will not be discussed but rather left behind the curtains of the MATLAB® implementation. This chapter will be a summary of the findings and conclusions of Pierre Apkarian and Dominikus Noll presented in [10].

Let the plant $P(s)$ be a real rational transfer matrix with the state-space representation:

$$P : \begin{cases} \dot{x} &= Ax + B_1 w + B_2 u \\ z &= C_1 x + D_{11} w + D_{12} u \\ y &= C_2 x + D_{21} w + D_{22} u \end{cases} \qquad P(s) : \begin{bmatrix} A & B_1 & B_2 \\ C_1 & D_{11} & D_{12} \\ C_2 & D_{21} & D_{22} \end{bmatrix}$$

where $x \in \mathbb{R}^{n_p}$ is the state, $u \in \mathbb{R}^{n_u}$ the control, $y \in \mathbb{R}^{n_y}$ the measured output, $w \in \mathbb{R}^{n_w}$ the exogenous input, and $z \in \mathbb{R}^{n_z}$ the regulated output.

Let the controller $K(s)$ be a real rational transfer matrix with the state-space representation:

$$K : \begin{cases} \dot{x}_K &= A_K x_K + B_K y \\ u &= C_K x_K + D_K y \end{cases} \qquad K(s) : \begin{bmatrix} A_K & B_K \\ C_K & D_K \end{bmatrix}$$

where $x_K \in \mathbb{R}^k$ is the state of K.

Given the plant $P(s)$ and controller space $\mathcal{K}$, a space of real rational transfer matrices $K(s)$ find the optimal solution $K^* \in \mathcal{K}$ of the optimization problem (4.2).

$$\begin{aligned} &\text{minimize } ||T_{w\to z}(P,K)||_\infty \\ &\text{subject to } K \text{ stabilizes } P \text{ internally} \\ &K \in \mathcal{K} \end{aligned} \tag{4.2}$$

Where $T_{w\to z}(P,K)$ is the closed loop performance channel (figure 4.12), $\mathcal{H}_\infty$-norm for a stable real transfer function $T(s)$, $||T(s)||_\infty = \max_{\omega\in\mathbb{R}} \bar{\sigma}(T(j\omega))$, and $\bar{\sigma}(M)$ is the maximum singular value of a complex matrix M.

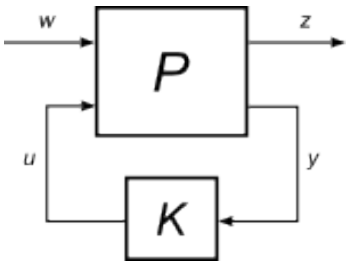

Figure 4.12: Closed loop system. w are disturbance inputs, u are controlled inputs, z are controlled outputs and y are measured outputs.

When $D_{22} = 0$, the closed loop transfer channel $T_{w\to z}(P,K)$ has the state space representation:

$$T_{w\to z}(P,K) : \begin{bmatrix} A(K) & B(K) \\ C(K) & D(K) \end{bmatrix}$$

where the state dimension is $n_p + k$ and

$$A(K) = \begin{bmatrix} A + B_2 D_K C_2 & B_2 C_K \\ B_K C_2 & A_K \end{bmatrix}.$$

If K stabilizes P internally, i.e. $A(K)$ is stable, then the closed-loop can be considered as a linear operator $T_{w\to z}(P,K)$ mapping the input $w \in L^2$ to the output $z \in L^2$ and the $\mathcal{H}_\infty$-norm is the L^2-L^2-operator norm, that is,

$$||T||_\infty = \sup_{w\neq 0} \frac{||Tw||_2}{||w||_2} = \sup_{w\neq 0} \frac{||z||_2}{||w||_2}.$$

For a closed-loop channel $w \to z$ the norm $\gamma = ||T_{w\to z}(P,K)||_\infty$ is the factor by which the energy of the input signal is amplified by the output. The optimization algorithm tries to find the controller $K^* \in \mathcal{K}$ for which the amplification factor γ is the smallest.

A controller K is called structured if the state-space matrices A_K, B_K, C_K, D_K depend smoothly on a design parameter vector θ varying in some parameter space $\mathbb{R}^n$ or in a constrained subset of $\mathbb{R}^n$. A controller structure $K(\theta)$ consists of four

smooth mappings $A_K(\cdot) : \mathbb{R}^n \to \mathbb{R}^{k\times k}$, $B_K(\cdot) : \mathbb{R}^n \to \mathbb{R}^{k\times n_y}$, $C_K(\cdot) : \mathbb{R}^n \to \mathbb{R}^{n_u\times k}$ and $D_K(\cdot) : \mathbb{R}^n \to \mathbb{R}^{n_u\times n_y}$.

Assuming that $K(\theta)$ is structured with parameter $\theta \in \mathbb{R}^n$ the closed-loop transfer channel $w \to z$ becomes:

$$T_{w\to z}(P, K(\theta)) : \begin{bmatrix} A(K(\theta)) & B(K(\theta)) \\ C(K(\theta)) & D(K(\theta)) \end{bmatrix}$$

and the $\mathcal{H}_\infty$-objective function in (4.2) becomes:

$$f(\theta) := ||T_{w\to z}(P, K(\theta))||_\infty = \max_{\omega\in\mathbb{R}} \bar{\sigma}\Big(C(K(\theta))(j\omega I - A(K(\theta)))^{-1}B(K(\theta)) + D(K(\theta))\Big)$$

a nonsmooth, nonconvex function not defined everywhere.

Its domain $D_f = \{\theta \in \mathbb{R}^n : f(\theta) < \infty\}$ contains the internally stabilizing set $D_s = \{\theta \in \mathbb{R}^n : K(\theta)$ stabilizes P internally$\}$. An optimization algorithm must search only this set and find the optimal parameters θ that minimize the $\mathcal{H}_\infty$-objective function.

Since such algorithms are exceedingly complex and transcend the scope of this thesis, reader is further referred to [11].

4.3.2 Modeling

First it is important to notice that a PI controller is a structured controller with state-space representation:

$$PI : \begin{cases} \dot{x}_K &= K_i e \\ u &= x_K + K_p e \end{cases} \qquad PI(s) : \begin{bmatrix} 0 & K_i \\ 1 & K_p \end{bmatrix}$$

dependent on the parameter vector $\theta = (K_i, K_p)$ and as such can be used in $\mathcal{H}_\infty$ optimization. MATLAB® function `hinfstruct` will be used to find the optimal parameters and the linear system is required as its input.

Figure 4.13 shows an augmented linear model of the system, rearranged to resemble the plant P. As it is shown on the figure 4.12, the controller K, in this case the PI controller, is connected to the plant so that the last input of the plant is the controller signal $u(t)$ and the last output is the control error $e(t)$. The rest of the inputs are reserved for "disturbances".

The idea behind this particular layout is quite simple. The $\mathcal{H}_\infty$ optimization that tries to minimize the amplification factor γ of the closed loop transfer function that

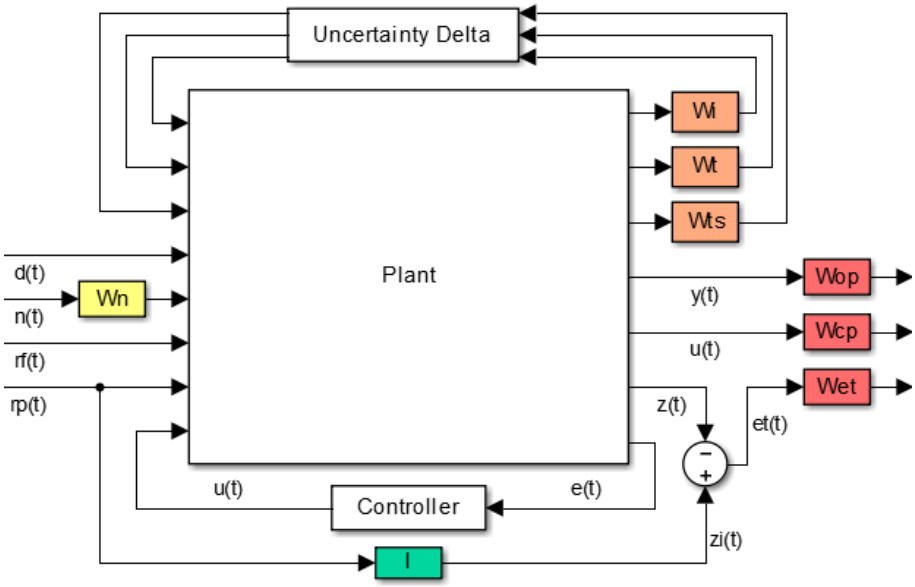

Figure 4.13: Augmented linear plant. Uncertain inputs together with $d(t)$, $n(t)$, $rf(t)$ and $rp(t)$ represent disturbance inputs, controlled input is $u(t)$ and the measured output is $e(t)$. The rest of the outputs are controlled outputs. Augmented system does not represent the real system but rather the adjusted system with added filters needed for control synthesis.

connects the disturbance inputs to the outputs of the plant will result in system least sensitive to the chosen disturbances.

First three inputs and outputs are connected to the model uncertainties which are removed from the plant. The uncertainties are described by the shaping filters (Wi, Wt, Wts) which also serve as a penalty weights for the plant outputs. In this way the interesting part of the uncertain dynamics is filtered out and penalised. If for example the uncertainty is the highest in the high frequency region, the filter will be a high pass amplifying that frequency range. The same filter from the perspective of the optimization algorithm represents the penalty function which by amplifying the high frequencies of the output signal forces the algorithm to find the solution in the low frequency range of the signal thus in effect minimizing the influence of the uncertainty.

Since most disturbances are in fact references like pressure reference $rp(t)$, flow reference $rf(t)$ or tubing identification static pressure parameter $d(t)$, and none of them is expected to change, no dynamic filter was added as a shaping weight to those signals. The only input shaping weight is Wn added to the sensor noise input $n(t)$ which, like mentioned earlier, describes the pump influence and high frequency sensor dynamics.

So far the weights were used to make the system robust against the uncertainties or disturbances, but other applications are possible. By adding penalty weight Wop

to the measured output $y(t)$ the performance channel can be tuned. The penalty weight Wcp connected to the control input $u(t)$ ensures the high frequency dynamics is penalised making the signal more stable for the actuators. Taking the reference through the ideal response system I and calculating the tracking error $et(t)$ using the controlled output of the system $z(t)$ and the ideal output $zi(t)$, loop shaping channel is formed. The penalty weight Wet associated with it is used to enforce the desired loop shape. These three weights are chosen by the system designer and are used for tuning the system behaviour. Often, there is a trade off between the stability of the control variable and the error tracking.

Augmented system used by the `hinfstruct` algorithm includes the input and outputs weights, the plant and the ideal system transfer function. Based on the choice of weights the parameters for PI controller are delivered. The resulting closed loop system is reported to be stable. Implementation details can be found in the code attached in the Appendix.

4.3.3 Simulation results

After obtaining the optimal parameters for the PI controller the system was simulated using the nonlinear model.

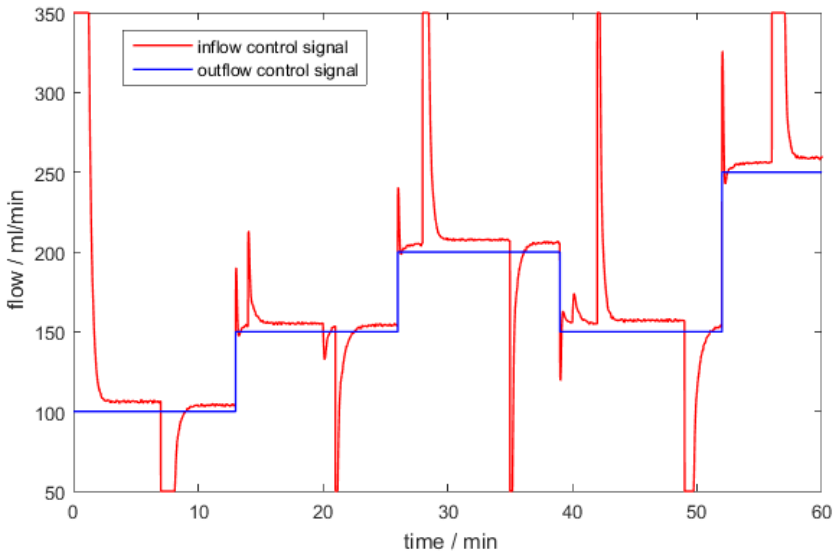

Figure 4.14: $\mathcal{H}_\infty$: control signal values. Outflow (blue) is the reference flow and the inflow control signal (red) spikes coincide with pressure reference changes and disturbance rejection.

As seen on the figure 4.14 the control signal is very stable with ripples less than 1 ml/min. This was one of the design choices in the optimization process, where the control signals high frequency dynamics were penalised. The optimal parameters for the PI controller thus give results of high control signal quality.

Measured pressure following its reference in figure 4.15 again shows good performance, but the greatest improvement is seen on the figure 4.16 showing cavity pressure and its reference. Stable, unlike the zone bang-bang result, without the overshoot like the tuned PI this response is a good example of the quality of robust control strategies.

With offset as low as 2 mmHg for the worst of conditions this results shows the best reference tracking as well as good disturbance rejection. Its greatest advantage is certainly the first order system like response. This is due to the fact that in parameter optimization the ideal response I that constituted the basis for error tracking was in fact a first order system.

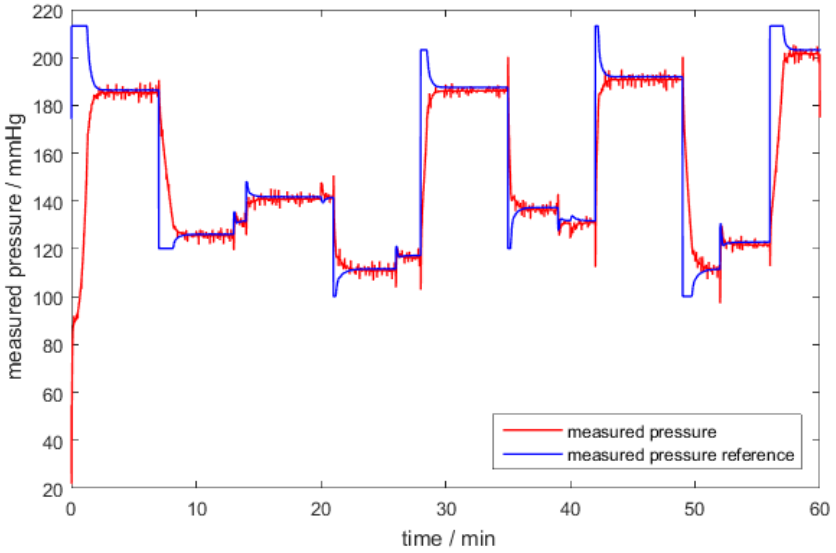

Figure 4.15: $\mathcal{H}_\infty$: measured pressure and reference. Measured pressure is the pressure visible on the sensors of the system consisting of the bladder pressure, pressure drop in tubing and disturbances.

Randomly sampling uncertainty values and running the nonlinear model simulation produces results shown on the figure 4.17. All the responses maintain their robust first order shape, are stable and show good reference tracking and disturbance rejection. There is no overshoot and the largest reference tracking error is 4 mmHg. These results are the best seen so far, though they have to be taken with caution. For the sampled uncertainties this system performs better than the one with the tuned PI or the zone bang-bang controller, and from this it can be generalised that it will give superior performance throughout the uncertain space.

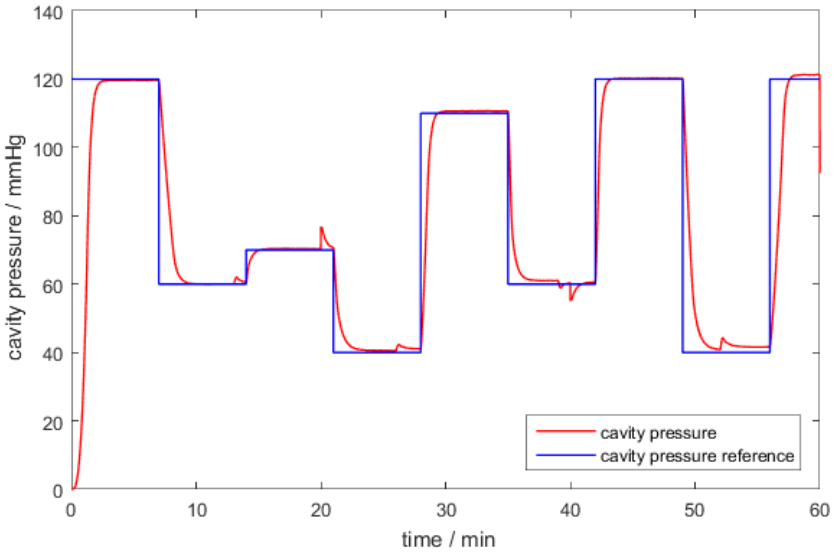

Figure 4.16: $\mathcal{H}_\infty$: cavity pressure and reference. Cavity pressure is not directly measured and can only be observed in the simulation environment. Small pressure spikes noticeable at times 20 min and 40 min are a consequence of internal bladder model disturbances. Spikes at times 13 min, 26 min, 39 min and 52 min are caused by flow reference changes.

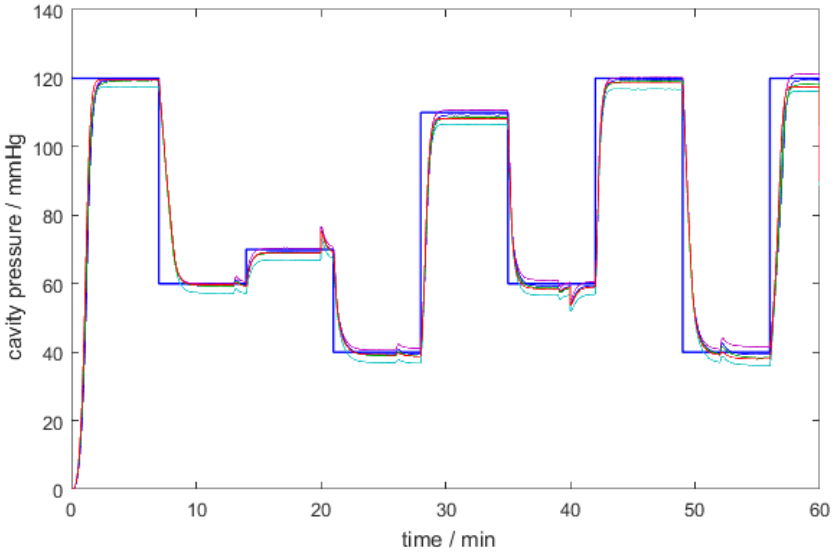

Figure 4.17: $\mathcal{H}_\infty$: system uncertainty influence on cavity pressure. Five different random simulations are presented.

4.4 Controller suggestion

After running simulation for all three controller variants the question of the best controller arises. From the figures 4.18 and 4.19 there is no doubt about the best

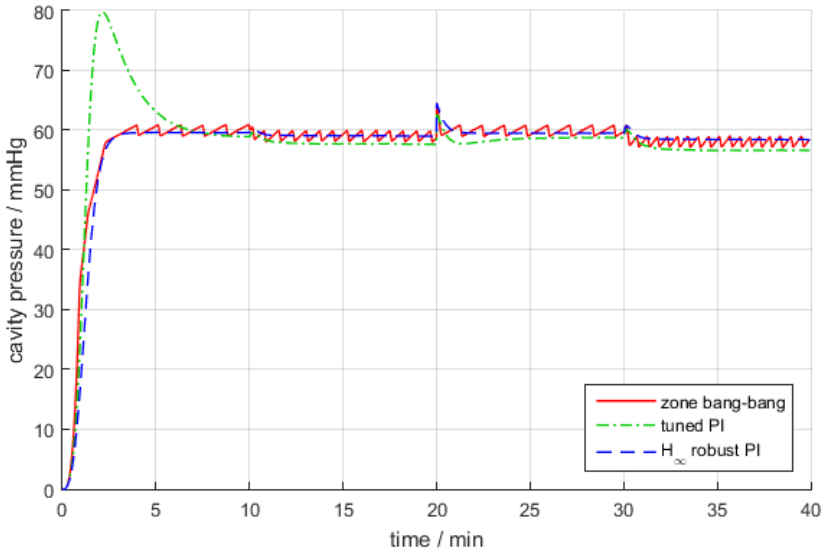

Figure 4.18: System responses to the 60 mmHg reference. Flow reference changes at times 10 min, 20 min and 30 min. Internal system disturbance occurs at 20 min.

performance controller. $\mathcal{H}_\infty$ robust controller has the most steady control signal, best reference tracking and overall the most stable performance. Problematic zone bang-bang control signal jumps make its response the most oscillatory one, and while tuned PI shows otherwise good performance the troublesome overshoot persists. Rising time is the shortest for the tuned PI but the settling time is the one to be considered in this situation and it is greater than 5 min. Zone bang-bang and the $\mathcal{H}_\infty$ robust controller are approximately the same in this respect. The control signal is bounded for all three controllers by 350 ml/min. Increasing this bound could lead to the faster performance, but also increases the uncertainty of the tubing identification and the prefilter reference error so it is not desirable.

Even though the $\mathcal{H}_\infty$ robust controller is the best in performance it is also the most complicated to synthesise. Modelling effort, complex mathematics and algorithms and choice of the weighting filters are the challenges of this method. Even if the final product is in the simple PI form, this controller synthesis requires specialist knowledge and a lot of time.

PI controller is much simpler. In some cases it does not even require the model of the system but can be tuned observing the responses. With the model, simulations can greatly improve the tuning of the parameters and lead to high quality responses.

Zone bang-bang is the simplest. Implementable as a state machine, with parameters chosen based on observing the system it provides the fastest solution.

The suggested controller in this case is after all the $\mathcal{H}_\infty$ robust controller. Despite its complexity, the benefit of high quality and robust performance coupled together with the insight into the system gained during the controller synthesis outweigh

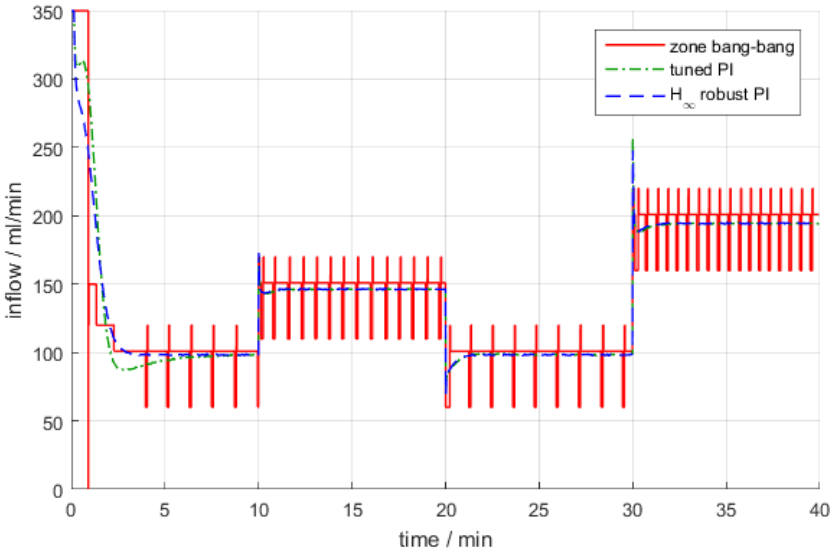

Figure 4.19: System control signals compared. Stable pressure reference of 60 mmHg is maintained.

the possible benefits of other studied controllers, especially in the case of uncertain systems.

5

Implementation

To test the conclusions reached in the previous chapters the test system was setup and the controllers implemented in the ENDO P®. The following chapter documents the implementation together with some observations and findings.

5.1 Test system setup

Test system consists of the ENDO P®, tubing and cassettes, container, 1.5 liter bottle, digital pressure sensor, computer, pressure gauge and a manual pump. Endoscope and the blood pressure monitor cuff were not included in the experiments.

Container is filled with water and it is used as the water source. After passing through the system, water returns to the container through the outflow tubing from the Patient cassette normally connected to the waste container.

Water bottle is used to model the cavity. It is upgraded with the digital pressure sensor connected to the computer, pressure gauge and the manual pump. The Day cassette outflow tube and the Patient cassette inflow tube, that are in the real system connected to the endoscope, are connected directly to the bottle in the test system.

In the running mode the ENDO P® is trying to maintain the set pressure and flow reference. The pressure in the bottle is observed on the gauge and recorded through the digital pressure sensor. Manual pump connected is used to increase or release the pressure when needed.

5.2 Bottle model

Since the cavity is replaced with the bottle, the separate mathematical model had to be found. Bottle was considered as a closed tank with the water inflow and outflow ports. No geometry was considered. As the volume of water in the bottle increases, the air, initially at the atmospheric pressure, is compressed which in terms leads to pressure rise. This dynamics can be summarised by the following equations.

$$V_{0,air} = V_{bottle} \tag{5.1}$$

$$\dot{V_{air}} = q_{out} - q_{in} \tag{5.2}$$

$$p_{bottle} = \frac{V_{0,air} p_{atm}}{V_{air}} - p_{atm} \tag{5.3}$$

Where V_{air} is the volume of air in the bottle, V_{bottle} is the initial bottle volume, q_{in} and q_{out} are the inflow and outflow, p_{bottle} is the pressure in the bottle and p_{atm} is the atmospheric pressure. Such bottle model was used in the nonlinear Simulink® model. Linearised version was also used to find the optimal controller parameters.

5.3 Controller comparison

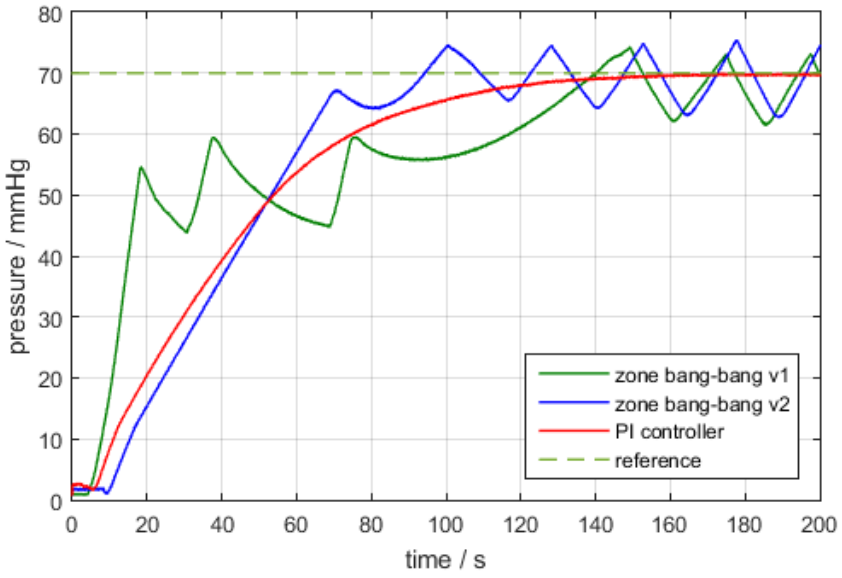

Figure 5.1: Test system responses with different controllers. The pressure reference signal is kept constant at 70 mmHg and the flow reference signal is kept constant at 200 ml/min. The saturation parameters for the PI controller are 300 ml/min and 50 ml/min. 0 mmHg pressure is not the starting pressure due to digital sensor imperfections and the dead time of each response is a consequence of human response time, since it takes some time from starting the pressure recording process to starting the ENDO P®.

On the test system three different controllers were compared. Two versions of zone bang-bang controller with different parameters and one PI controller. Parameter values for the PI controller were found through $\mathcal{H}_\infty$ optimization method presented in chapter 4 and than tested out on the nonlinear system model. Further tuning was done manually based on the intuition gained from the optimization and the model.

Considering the figure 5.1 the most stable response is the one of the PI controller. The zone bang-bang in both cases has the oscillations of magnitude 5 mmHg which is not insignificant. Rise times of both controllers are similar so the PI controller is a better choice due to response stability.

Comparing the recorded responses from the test system and the simulated responses from the test system model some differences can be observed, but in general, as shown on the figure 5.2, the model is a good representation of the system behaviour. Small discrepancies can be attributed to unidentified tubing dynamics and the considerable simplification of the mathematical model.

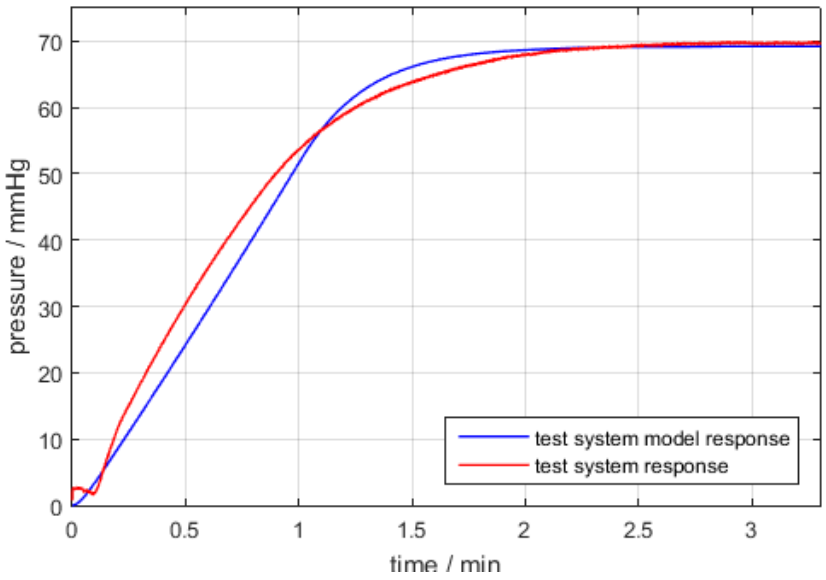

Figure 5.2: Test system response compared to the simulation. The pressure reference signal is kept constant at 70 mmHg and the flow reference signal is kept constant at 200 ml/min. PI controller is used.

Finally some conclusions can be drawn from the implementation results. Despite the simplicity of the zone bang-bang, if the model of the system can be derived, PI controller is a better choice. In the simulations presented in the chapter 4, the problem of zone bang-bang oscillations was underestimated and in the real implementation this presents a significant problem which could not be solved even after some parameter adjustments. On the other hand, PI parameters derived using the $\mathcal{H}_\infty$ optimization were not the best set of parameters found. Only after manual tuning did the PI controller show its full potential. What can be concluded from that is that the $\mathcal{H}_\infty$ optimization is too reliant on the model. It can be considered as a starting point, but should be approached with a grain of salt in the case of the real system. Regardless, it is invaluable for building the intuition of the system.

The control signal values were not recorded and thus cannot be shown. What was noticed during the tests is that the PI again showed the superior performance. Once

the system settled the control signal was almost constant, while in the case of the zone bang-bang it kept oscillating to manage the reference tracking.

Unfortunately, due to the time constraints, only limited amount of tests could be carried out. This is certainly one of the points that needs to be addressed in further work. Different bottle sizes and different bottle materials should be tested out. Test duration should be increased to better match the surgery conditions and the changes to reference pressure and flows should be introduced. Further tuning of the PI controller should also be considered.

6

Graphical User Interface design

The graphical user interface is an important part of ENDO P® software. It should follow the flow of the surgery, be intuitive and clear. It should offer as much relevant information as possible to the surgeon, be safe so that unintended or misplaced touches cannot initiate unwanted behaviour and it should also be easy to operate in terms that minimal amount of actuation is necessary. Design should find a good balance between conflicting requirements of safety and ease of use. It should be visually attractive and the information should be presented in a way that relevance of information is also noticeable making the more relevant information easier to notice. Following chapters present the flow of the surgery conducted using ENDO P® and the design choices explained on each of the screens.

6.1 Procedure flow

To start the surgery with the ENDO P® several preconditions need to be met. The flow of the surgery will assume usage of EBI™ (empty bag indicator) and ENDO H® (heater bag).

Preconditions are the following:

- ENDO P® is in working condition and turned on,
- foot pedals are connected and in working order,
- sound alarm is audible,
- EBI™ is connected and in working order,
- blood pressure monitor cuff is connected,
- height values for the hydrostatic pressure calculations are measured and stored into the device.

Preparation for the specific surgery is then carried out. Nurse installs the two irrigation fluid bags on the EBI™. Fluid bags are then connected to the Day cassette

that was installed at the first surgery of the day along with the ENDO H®. The Day cassette together with the related tubing is then primed, and the fluid once in the system is prevented from leaking out by a clamp nurse closes at the end of the outgoing tube from the Day cassette.

From this point on the ENDO P® should be in standby mode. It should offer the possibility of automatic height calibration and surgery selection. Nurse can preform these actions but can also choose to wait for the arrival of the surgeon.

Automatic height calibration is an additional procedure that confirms the hydrostatic pressure calculated previously from the entered height difference. In this procedure pumps pressure sensors are used to directly read out the hydrostatic pressure of irrigation fluid column at the height of the operating table.

Before the start of the surgery Patient cassette needs to be installed. Patient cassette tubing needs to be connected to the endoscope. Outgoing end of the Patient cassette tubing is placed in the waste collector. Part of the tubing is connected to the outgoing tubing from the Day cassette on one end and to the endoscope on the other. Clamp is then opened and the endoscope can be primed. It is important that Patient tubing installation is done by the sterile nurse.

Once the surgeon is in the room, height of the operating table can be adjusted and automatic height calibration redone. Surgery, if not selected before, should now be selected. With all the preparations ready, surgery starts with surgeon inserting the endoscope in the cavity. ENDO P® is activated by entering the running mode.

Once in the run mode, the priming of the bladder is carried out and when the desired pressure is reached ENDO P® control algorithm maintains it. During all this time surgeon can see the pressure and the flow in the cavity on the display. Blood pressure measurements are taken regularly and the set-point pressure is recalculated and applied.

During the surgery the surgeon can increase or decrease the set-points at will. The standby mode can also be reentered to preform the height calibration again, to change the procedure type or finish the surgery.

ENDO P® interrupts the surgery without surgeon command in cases of errors such as:

- EBI™ senses no more irrigation fluid in the bags,
- pressure sensors sense dangerously high pressure,
- ENDO P® detects an internal failure.

After appropriate measures have been taken surgery can continue. Surgery finishes when the pump exits the running mode, end procedure is initiated by the surgeon and the endoscope is evacuated from the patient.

6.2 Design choices

Design choices presented in this chapter are not necessarily used in the final ENDO P® user interface screens. Flow, graphical elements, layout and color scheme of the shown figures might slightly vary in the final version. The screens were designed and drawn in Inkscape [2].

Diagnostics screen was created to aid the process of identifying possible failures on ENDO P® start. It is used to check for possible failures in inputs and outputs (pedals, speakers and EBI™). It is intended to guide the user to check the hardware issues that cannot be detected otherwise. These actions are expected to be performed only on start-up i.e. once a day.

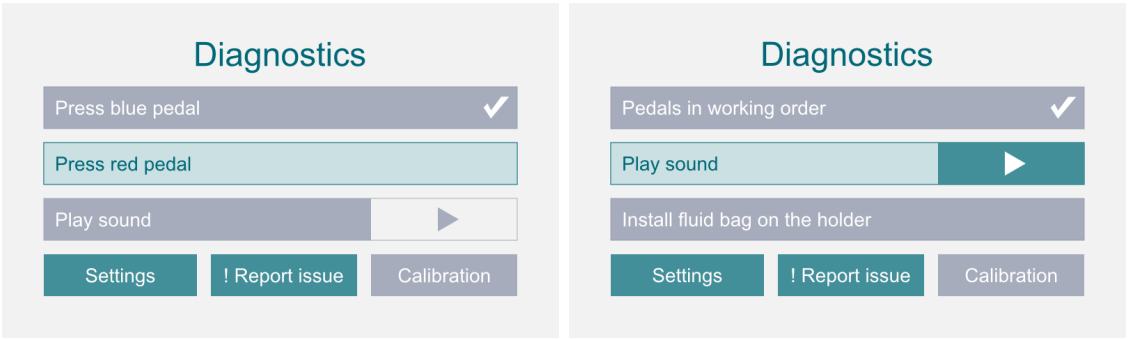

Figure 6.1: Diagnostic screen. Left: Screen expecting the operator to preform the highlighted action. Right: Screen prompting the operator to tap the play button on the screen.

Figure 6.1 shows the diagnostic screen layout. The expected action is highlighted, the successfully finished actions are checked off and coming actions are listed underneath the expected one.

The graphical element arrow represents the play button. On press, the sound is played through the speakers. User is prompt to confirm to have heard the sound or use the *!Report issue* button to note the malfunction.

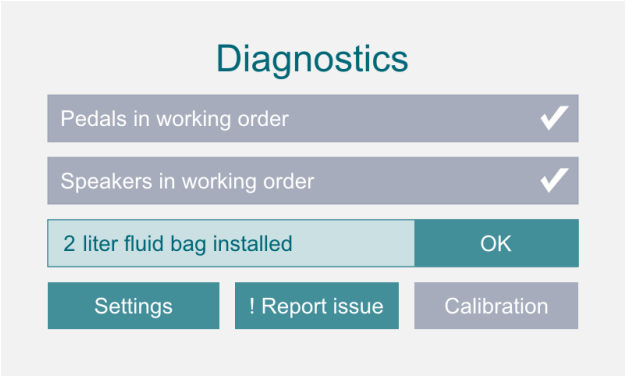

Figure 6.2: EBI™ Diagnostic screen addition.

In case of EBI™ use, additional part of diagnostic screen prompts the user to install the fluid bag on EBI™ and after measuring, feeds back the bag size (1 liter or 2 liter) to user for confirmation.

From the diagnostic screen, user can enter settings to get the instructions in a different language or to increase volume or screen brightness.

Settings screen is used to set the user preferences for the ENDO P® interface. It enables user to choose the language by continuing to language selection screen. It also enables user to choose between 5 levels of volume and 5 levels of screen brightness or return to the diagnostics. Language selection enables user to select between 6 languages and return to the settings screen.

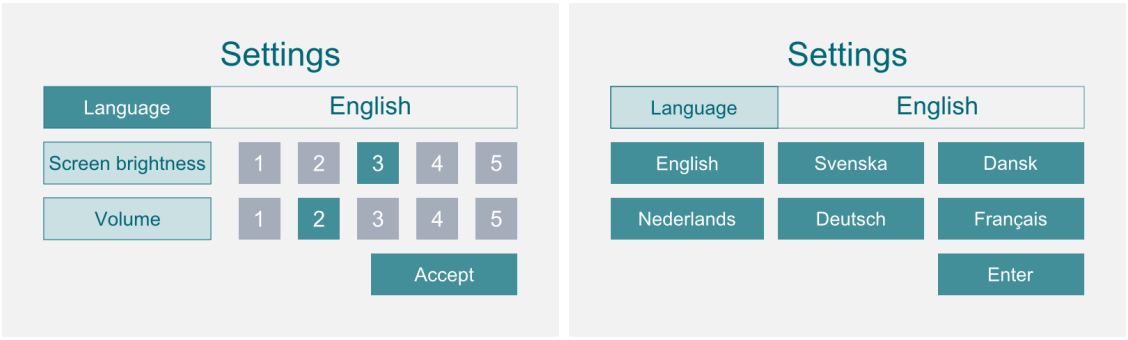

Figure 6.3: Settings screen. Left: By taping on the numbers the screen brightness and system volume can be adjusted. Right: Language selection part of the settings screen.

Once all the diagnostics actions are completed successfully and ENDO P® has registered the user preferences it is possible to continue to the manual height calibration screen.

Figure 6.4: Manual height calibration screen. Left: Height to patient or height to ENDO P® can be selected. Right: The selected and highlighted is entered by tapping on numbers.

Manual height calibration screen allows the user to choose patient height or ENDO P® height for input or to accept preset values and continue to the main screen. It serves to calculate hydrostatic pressure based on difference in height. By pressing

enter, inputted value is stored and the screen returns to the previous layout of manual height calibration screen.

Main screen is intended to be central screen which allows for different actions such as priming the tubing, procedure selection, automatic height calibration and also serves as standby screen during the procedure.

Main screen layouts are divided to before surgery screen and during surgery screen. Functions of those screens are the same, just buttons relating to start/continuation of and finish of the surgery are different. Figure 6.5 shows the before surgery layout of the main screen.

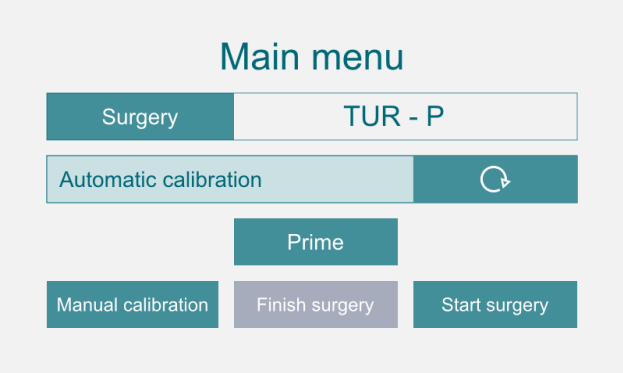

Figure 6.5: Main screen. Central screen leading to surgery selection, height recalibration, priming and surgery run screen.

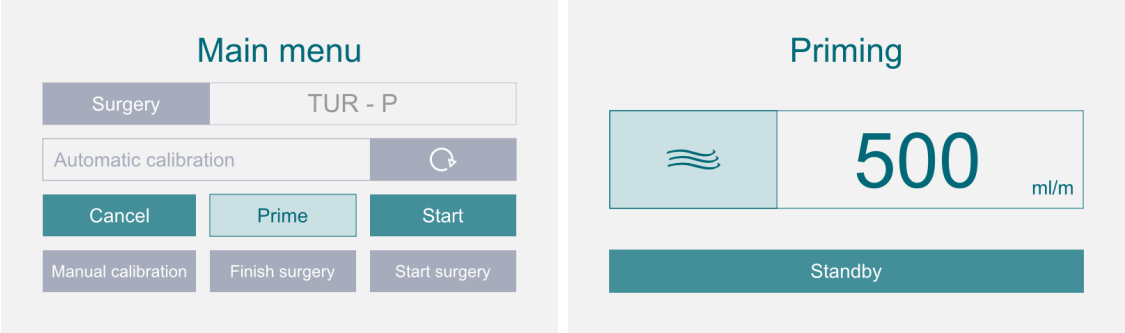

Figure 6.6: Priming procedure screens. Left: Safety screen preventing an unintended start of the priming procedure. Right: Priming procedure screen displaying the current flow.

After the prime button is pressed, prime options part of the main screen is activated. It requests additional confirmation before continuing to the priming screen. The priming can also be canceled to return to the main screen.

Additional confirmation was done in order to provide greater safety of operation. Priming procedure is carried out at high flow rate and has only high pressure detection part of the main algorithm. Additional confirmation was done to reduce the likelihood of unintentional start of tubing priming during the surgery.

Priming screen is used to display the flow while priming the tubing. On standby it returns to main screen. Icon showing three curves represents the flow.

In the main screen after the rotating arrow representing the re-calibration is pressed and automatic height calibration procedure is initiated the automatic height calibration screen appears. It displays the numbers representing height from the ground at which the opened tubing is held. Once the blue pedal is pressed (actuation of the blue pedal is suggested by blue line around the numbers) the last number is stored as valid and the screen returns to main menu screen.

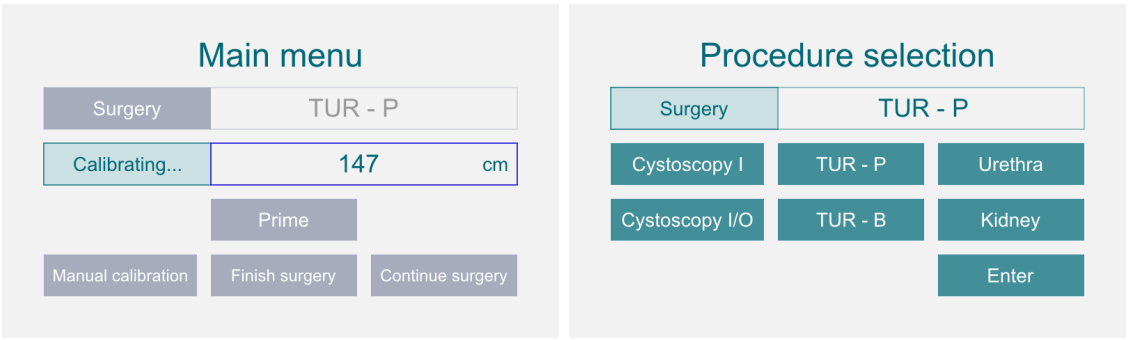

Figure 6.7: Automatic height calibration and procedure selection screens. Left: Automatic height calibration screen displaying the currently measured patient height. Right: Procedure selection screen. Procedures are selected by taping the wanted procedure button.

Procedure selection screen is entered from the main screen when the surgery button is tapped or when user attempts to start a surgery without selecting the procedure. On first entry, it is necessary to select the procedure; otherwise the screen does not allow the user to return to main screen. Aside from tapping on the procedure name, user also has to confirm it by tapping Enter.

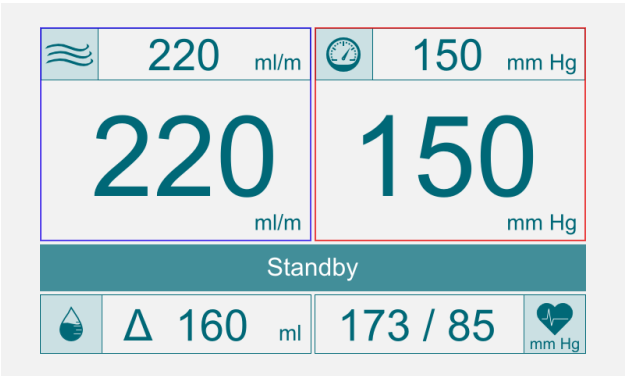

Figure 6.8: Run screen. Screen visible during ongoing surgery. Standby is the only active button. Values are displayed to inform the surgeon about the surgery conditions.

Run screen is visible during the surgery. Upon actuation of Standby button it returns to main menu screen. Icon showing three curves represents flow, gauge

represents pressure, drop with measurement represents differential volume and the heart represents blood pressure measurement. Blue square around flow values relates the blue pedal actuation to flow control and red square around pressure values relates the red pedal actuation to pressure control.

From left to right and from up to down screen displays following values: flow set-point value, pressure set-point value, actual flow value, actual pressure in the cavity value, differential volume calculation and blood pressure measurement. The largest numbers represent the measures of most interest. The set-points are conveniently placed just above the controlled measures.

7

Conclusion

The ENDO P® is without a doubt a great innovation. As the results of the first clinical trials show, surgeries are made faster (up to 30% time saving), much less fluid is used, a minimum amount of irrigation fluid is absorbed by the patient and the visibility throughout the surgery, even with the lowest of pressure and flow set-points, is excellent.

One of the most significant results is the ability to extend the surgery at need. Without such a device, the time for surgery was constrained to avoid the occurrence of TUR-P syndrome. That meant not all the patients could be treated with such minimally invasive method.

Using the ENDO P® time is no longer a limiting factor. Size of the prostate gland is no longer an issue, and all the cancerous tissue can be removed in just one surgery. All the benefits of the minimally invasive procedures for the patients, such as less tissue damage, less bleeding and faster recovery are, by the so far observed results, further enhanced by the ENDO P® usage.

The study of the ENDO P® system in the sense of pressure and flow control is quite challenging. This thesis brought forth a model of the system together with the suggestion for the control algorithm. The issue from the beginning was the uncertainty of the biological system model which is often a problem when designing medical devices featuring new functions. Lack of data, methods and sensors to identify all the system behaviours resulted in a highly uncertain model.

One significant problem was the pressure drop in tubing which could not be derived mathematically. System identification was performed, but due to the lack of proper sensors, only the static model was found. Finding the dynamic model through a black box approach should be done as an extension to this work, even if the dynamics would not be able to capture the moving geometry of the system, they would represent an improvement from the current case.

Another problem was the bladder model. Being a biological system, dependent on biological parameters different from one patient to the other, there was no way to model this part without uncertainty. In the modeling process the greatest problem was finding the compliance parameter which most of the literature identifies differently and without much success.

The method taken to model the bladder behaviour in this thesis was dependent on quite few assumptions that may prove not to be true. This in term would influence the $\mathcal{H}_\infty$ optimization algorithm. In the future it is necessary to aquire more intuition about the system through the ENDO P® use and collect as much data as possible from the real surgeries. This would allow for the model upgrade, resulting in better overall results.

The controllers suggested and compared were chosen based on the ease of implementation. As an surgical instrument, the main quality of the ENDO P® should be reliability and that should also be the main quality of its control algorithm. The simple state machine or the tested and tried PID controller are thus the best options.

Zone bang-bang proved to be a quick and versatile solution. Without the need of a model, this solution offered reasonable performance quality. Its greatest drawback was the unsteady control signal that caused oscillation in the system output as well.

PI controller scheme offered a good trade-off between just observing system response and building the complex model. With the simple linear model and some intuition about the system, parameters that provided a stable output were found. The greatest problem of the PI solution was in the transition range of the system response. Overshoot was present and settling time significantly higher than that of the other two algorithms.

And finally $\mathcal{H}_\infty$ structured robust controller was found. The structure of the familiar PI controller was used. This method of controller synthesis was the most complicated one, requiring an elaborate model of the system, specialist control knowledge and advanced optimization algorithms solving software. Taking into account the system uncertainties this method provided the best results in terms of performance, robustness and stability. Its only drawback was the complexity of control synthesis and the reliance on the model.

The $\mathcal{H}_\infty$ structured robust controller was in the end suggested by this thesis as the best choice for this application because it was the only method that minimised the influence of the uncertainty in the highly uncertain system. This particular method shows great promise because of its potential to close the gap between the academic control community and practical control algorithm implementation. Hidden behind the simple form, the powerful optimisation algorithms enable the best responses coupled with high reliability and easy implementation. This could be the best way of meeting the control requirements for the complex uncertain biological systems.

The initial GUI design presented in the chapter 6 of the thesis was made considering the procedure flow, safety of operation and ease of use. The first feedback from the users is positive, though some improvements will need to be done to achieve the design goals. Future work in this area should include consideration for the better utilization of the pedal inputs as well as inclusion of more information in the run screen.

Bibliography

[1] Bonvisi AB online. Retrieved: 2015-06-01.
Accessible at: http://www.bonvisi.com/

[2] Inkscape online. Retrieved: 2015-06-01.
Accessible at: https://inkscape.org/en/

[3] MATLAB® online. Retrieved: 2015-06-01.
Accessible at: http://se.mathworks.com/products/matlab/

[4] Simulink® online. Retrieved: 2015-06-01.
Accessible at: http://se.mathworks.com/products/simulink/

[5] O'Donnell A. M., Foo I. T. H., *Anaesthesia for transurethral resection of the prostate*, (2009), Continuing Education in Anaesthesia, Critical Care & Pain, Volume 9, Issue 3 pp. 92-96, first published online May 4, 2009, Retrieved: 2015-05-29.
Accessible at: http://ceaccp.oxfordjournals.org/content/9/3/92.full

[6] Mangan R., Destrade M., *Gent models for the inflation of spherical balloons*, (2015), International Journal of Non-Linear Mechanics, Special Issue in Honour of Alan Gent 68 pp. 52-58, Retrieved: 2015-04-21.
Accessible at: http://www.maths.nuigalway.ie/d̃estrade/publications/

[7] Mooney M., *A theory of large elastic deformation*, (1940), Journal of Applied Physics 11, pp. 582–592.

[8] Osborne W.A., *The elasticity of rubber balloons and hollow viscera*, (1909), Proceedings of the Royal Society of London. Series B, Containing Papers of a Biological Character 81 (551): pp. 485–499, Retrieved: 2015-02-15.
Accessible at: https://archive.org/details/philtrans06128149

[9] Hole, J. W., *Human Anatomy and Physiology*, (1987), William C. Brown, Burr Ridge, U.S.A.

[10] Apkarian P., Noll D., *The H_∞ control problem is solved*, (2012), Retrieved: 2015-04-15.
Accessible at: http://www.math.univ-toulouse.fr/ñoll/PAPERS/solved.pdf

[11] Apkarian P., Noll D., *Nonsmooth H_∞-synthesis*, (2006), IEEE Transactions on Automatic Control vol. 51, no. 1, pp. 229-244.

[12] Pipe Flow Calculation online. Retrieved: 2015-03-10.
Accessible at: http://www.pipeflowcalculations.com

[13] Wahl et al., *Measurement of bladder compliance can be standardized by a dimensionless number: clinical perspective*, (2004), BJU International, Volume 94, Issue 6, pp. 898–900, Article first published online: 8 OCT 2004
Accessible at: http://onlinelibrary.wiley.com/

[14] Toppercer et al., *Compliance of the bladder: An attempt to establish normal values*, (1979), Urology, Volume 14, Issue 2, pp. 204-205.

[15] Warsaw University of Technology - Electrical Engineering, Institute of Control and Industrial Electronics online. Retrieved: 2015-06-4.
Accessible at: http://www.isep.pw.edu.pl/ZakladNapedu/lab-ane/anti-windup

[16] Lockheed Martin Skunk Works, Lockheed Martin Tactical Aircraft Systems, Honeywell Technology Center, *Application of multivariable control theory to aircraft control laws*, (1996) pp. 156-181.

[17] Åström K.J., Murray R. M., *Feedback Systems: An Introduction for Scientists and Engineers*, (2008), Princeton University Press, New Jersey.

[18] Frisk, D., *A Chalmers University of Technology Master's thesis template for LaTeX*, (2014), Unpublished.

A

Appendix

MATLAB® script: modelparameters.mat

```
Tsim = 100;
load('cavitymap.mat')
a = 20;
atm = 760;
x20 = 2000;
smod = 'linearmodel';

pressure = 60;
ref_pressure_vector = [120 60 70 40 110 60 120 40]; %mmHg
ref_pressure_vector_sample_time = 7;    %min
outflow = 100; %ml/min

ref_outflow_vector = [100 150 100 200];
ref_outflow_sample_time = 10;

height_diff = 20; %cavity 20 cm higher than patient
cmH2OtommHg = 0.73556;
spressure = 40 + height_diff*cmH2OtommHg;

c = ureal('c',0.7250);
c.range = [0.25 1.2];
p = ureal('p',30);
p.range = [20 40];
val_all = [];
s = tf('s');

A = 0;
B = [1 -1];          % u_in - u_out
C = c;
D = 0;
```

```
Ad = 1/(s/p+1);      % actuator dynamics
Pd = ss(A,B,C,D);    % process dynamics
Sd = tf(1);          % sensor dynamics

% prefilter based on identified static relations
A = 0;
B = [0 0];
C = 0;
D = [0.11 1];

F = ss(A,B,C,D);

% unmodeled input dynamics
Di = ultidyn('Di',[1 1]);
Wi = tf(0.05);
pd = ureal('pd',0.015);
pd.range = [0 0.02];

% unmodeled output dynamics (tubes)
T = tf(0.11);
Dt = ultidyn('Dt',[1 1]);
Wt = makeweight(0.2,10,20);
Dts = ureal('Dts',0);
Dts.range = [-1 1];
Wts = tf(0.05);

% weights
Wn = makeweight(0.1,100,2.5); % simulates noise dynamics
Wcp = makeweight(0.01,50,15);% penalize control signal
Wop = makeweight(10,4,0.1);% penalize output performance
Wet = makeweight(500,0.1,0.01);% penalize the tracking error

% Controller
Kc = ltiblock.pid('Kc','pi');
Kc.Kp.Value = 1;
Kc.Ki.Value = 1;
k = 10;
Kf = tf(k,[1 k]);

% Ideal response
I = 1/(s/5+1);
```

```
%% ------------------------------------  SIMULINK APPROACH
% Create a tuning structure from the model
SYS = slTuner(smod,{'Kc'});
setBlockParam(SYS,'Kc',Kc);

addPoint(SYS,{'d0','d1','d2','d3','d4','d5','d6',...
    'e1','e2','e3','e4','e5','e6'});
ASYS = getIOTransfer(SYS,{'d0','d1','d2','d3','d4',...
    'd5','d6'},{'e1','e2','e3','e4','e5','e6'});

% Structured H infinity robust control (PI + filter)
rng('default')
opt = hinfstructOptions('Display','final','RandomStart',10);
[TR,gammas,info] = hinfstruct(ASYS,opt);
pid(TR.Blocks.Kc)
Kc = TR.Blocks.Kc;


%% -------------------------------    UNCERTAINTY SIMULATION

szbb = 'nonlinearmodel';
uvars=ufind(szbb);
for i=1:1;
       val_all = usample(uvars);
       sim(szbb,Tsim);
end
```